Effects of Ozone-Climate Interactions on the Long-Term Temperature Trend in the Arctic Stratosphere

Siyi Zhao[1], Jiankai Zhang[1*], Zhe Wang[1], Xufan Xia[1], Chongyang Zhang[1]

[1]College of Atmospheric Sciences, Lanzhou University, Lanzhou 730000, China

5   *Correspondence to*: Jiankai Zhang (jkzhang@lzu.edu.cn)

Abstract. Using reanalysis datasets and the Community Earth System Model (CESM), this study investigates the effects of ozone-climate interactions on the Arctic stratospheric temperature changes during winter and early spring. Before 2000, the Arctic stratospheric temperature increased significantly in early winter (November and December), which is primarily due to ozone-climate interactions. Specifically, the increasing trend in ozone during this period leads to longwave radiation cooling

10   in the stratosphere. Meanwhile, ozone-climate interactions lead to a stratospheric state that enhances upward wave propagation and the downwelling branch of the Brewer-Dobson circulation, which in turn adiabatically warms the stratosphere and offsets the direct longwave radiative cooling of the ozone. Additionally, enhanced upward wave propagation can lead to an equatorward shifting of the stratospheric polar vortex toward the eastern coast of Eurasia during November. In contrast, during late winter and spring, cooling trends in the Arctic stratosphere are predominantly driven by the reduced shortwave radiation

15   heating associated with stratospheric ozone depletion. This study highlights the impacts of ozone-climate interactions on the long-term trend in the Arctic stratospheric temperature.

Keywords: stratospheric temperature, ozone-climate interactions, ozone-circulation feedback, stratospheric polar vortex, planetary wave activity

1 Introduction

20   The stratospheric ozone layer plays an important role in global climate change (Son et al., 2008; Smith and Polvani, 2014; Xia et al., 2016; Xie et al., 2018; Hu et al., 2019a; Sigmond and Fyfe, 2014; Chiodo et al., 2021; Ivanciu et al., 2022; Friedel et al., 2023). Its absorption of solar ultraviolet (UV) radiation, along with its strong infrared radiation (IR) absorption and emission around the 9.6 μm band, is crucial for the Earth's energy balance and the thermal structure of the atmosphere (de F. Forster and Shine, 1997). The annual global mean radiative forcing of stratospheric ozone during the strongest ozone depletion period

25   (1979–1996) is relatively small (-0.22 ± 0.03 W/m^2; de F. Forster and Shine, 1997) compared to that of CO_2 (2.16 ± 0.25 W/m^2; IPCC, AR5, 2014). However, in addition to the direct radiative forcing mentioned above, stratospheric ozone can also significantly impact atmospheric temperature through the ozone-climate interactions, which involve chemical-radiative-dynamical coupling processes (Dietmüller et al., 2014; Nowack et al., 2015). For instance, neglecting interactive stratospheric

chemistry and considering only ozone's direct radiative effect in climate models result in 20% overestimation of surface temperature in scenarios with the quadrupled CO_2 concentrations (Nowack et al., 2015). A similar overestimation of surface temperatures can also be found in the study of Chiodo and Polvani (2016). Additionally, Rieder et al. (2019) demonstrated that ozone-climate interactions are important for accurately capturing stratospheric temperature variability in models. However, some studies, such as Marsh et al. (2016), suggested that ozone-climate interactions have limited influences (approximately 1%) on climate sensitivity. Therefore, whether the ozone-climate interactions have significant influence on temperature variability is still unclear.

The ozone-climate interaction is complex, especially in the polar stratosphere. It involves different feedback mechanisms that vary across seasons. In winter, although solar radiation in the Arctic regions is absent, ozone can still absorb and emit longwave radiation. Seppälä et al. (2025) pointed out that a reduction in stratospheric ozone could directly lead to stratospheric warming. This longwave radiative warming may influence the strength of the Arctic polar vortex (Hu et al., 2015), further modulating the transport of ozone-rich air from mid-latitudes to the Arctic polar regions (Zhang et al., 2017). In addition, the Arctic ozone can modulate the planetary wave activity, which further influences Arctic stratospheric temperature via wave-mean flow interactions in winter (Nathan and Cordero, 2007; Albers and Nathan, 2013; Hu et al., 2015). Thus, Arctic stratospheric ozone affects stratospheric temperatures through its longwave radiative effects and dynamical processes during winter. In late-February and early spring, as solar radiation reaches high latitudes, the polar regions become warm compared to winter and the stratospheric polar vortex is weakened. However, from the perspective of climate, the increase in ozone depleting substances (ODSs) in the 20th century leads to springtime stratospheric ozone depletion and decreased absorption of shortwave radiation, which cools the Arctic stratosphere and strengthens the polar vortex (Friedel et al., 2022a). This results in reduced wave propagation towards the lower stratosphere and thereby a colder Arctic stratosphere (Coy et al., 1997; Albers and Nathan, 2013; Haase and Matthes, 2019). On the one hand, the strengthened Arctic polar vortex decreases ozone transport to the polar regions, further reducing ozone concentrations. On the other hand, a colder Arctic stratosphere facilitates the formation of polar stratospheric clouds (PSCs). PSCs provide sites for heterogeneous reactions. The reactions convert stable chlorine reservoir species into active chlorine, then catalytically destroys ozone (Solomon et al., 1986; Feng et al., 2005a, 2005b; Calvo et al., 2015). Therefore, the ozone-climate interactions in winter and spring involve different and complex chemical-radiative-dynamical feedback processes, which operate on different timescales (Tian et al., 2023).

The Arctic plays a crucial role in the global climate system, and its temperature changes have profound implications for global climate patterns (Cohen et al., 2014; Serreze and Barry, 2011; Overland et al., 2016). In recent decades, the Arctic long-term temperature trends are not only driven by a range of external factors such as sea ice, greenhouse gas emissions (GHG), and aerosols (IPCC, AR6, 2021; Shindell and Faluvegi, 2009; Screen and Simmonds, 2010), but also influenced by natural variability in the climate system. During the period from 1950 to 2000, in late-winter, a negative trend in stratospheric temperature is observed in the Arctic regions, which is associated with the weakening of wave activity (Randel et al., 2002;

Zhou et al., 2001; Hu and Tung, 2003). On the other hand, the temperature trends in early and mid-winter (November-January) are opposite to those in late winter from 1980 to 2000 (Bohlinger et al., 2014; Young et al., 2012). Most previous studies focused only on the role of dynamical processes in the seasonal difference in temperature trends (Newman et al., 2001; Hu and Fu, 2009; Young et al., 2012; Ossó et al., 2015; Fu et al., 2019). However, these long-term trends in Arctic temperatures are not fully explained by dynamical processes. A recent work by Chiodo et al. (2023) has explored the impact of long-term ozone trends on the temperature in the Arctic, providing valuable insights into the ozone-climate interactions. Notably, the Arctic ozone layer has also undergone significant changes over the past 40 years (WMO, 2018). The ozone layer experienced significant depletion after the Industrial Revolution (Farman et al., 1985) and has been recovering slowly in the 21st century as ODSs is decreased (WMO, 2018; Newman et al., 2007; Chipperfield et al., 2017). Additionally, the influence of ozone-climate interactions on temperature in polar regions differs across seasons (Tian et al., 2023). Therefore, it is worth investigating whether Arctic ozone trends and their climate interactions can explain the long-term trends in Arctic temperature across different seasons.

This study focuses on the historical long-term trends in the Arctic stratospheric temperature during winter and spring, with a particular emphasis on the role of ozone-climate interactions. Specifically, we seek to answer the following questions: (1) What are the observed trends in Arctic stratospheric temperature and ozone concentrations over recent decades? (2) How do ozone-climate interactions contribute to these trends? (3) What mechanisms drive the seasonal differences in these trends? By addressing these questions, this study aims to enhance our understanding of the role of ozone-climate interactions in long-term Arctic stratospheric changes and their implications for future climate projections. Section 2 outlines the data, methodologies, and climate model experimental designs employed in this study. Section 3 presents the observed trends in temperature and ozone concentrations over the Arctic stratosphere, and Section 4 explores the underlying physical processes. Finally, section 5 summarizes the conclusions and discusses future directions.

2 Data, methods and experimental configurations

2.1 Data

The European Centre for Medium-Range Weather Forecasts (ECMWF) v5 reanalysis dataset (ERA5; Hersbach et al., 2020) from 1980 to 2020 is used in this study. The horizontal resolution of this dataset is $1°\times1°$ (latitude $\times$ longitude) and there are 37 vertical levels ranging from 1000 to 1 hPa. The daily and monthly mean results are derived from the 3-hourly ERA5 reanalysis dataset. We also used daily meteorological data obtained from the NASA Modern-Era Retrospective Analysis for Research and Applications version 2 (MERRA2) product (Gelaro et al., 2017), which has a horizontal resolution of $1.25°\times 1.25°$ (latitude $\times$ longitude), and 42 pressure levels in the vertical direction extending from 1000 to 0.1 hPa from 1980 to 2020. The meteorological fields used in this study include daily mean horizontal winds, temperature, geopotential height and ozone.

 2.2 Methods

2.2.1 Diagnosis of wave activity

2.2.1.1 Elisassen-Palm flux

The Elisassen-Palm (E-P) flux (Andrews et al., 1987) is used to diagnose the propagation of waves in the vertical and meridional directions and is calculated as follows:

$$F_\phi \equiv \rho_0 a cos\phi \left(\frac{\overline{u_z}\overline{v'\theta'}}{\overline{\theta_z}} - \overline{u'v'} \right)$$ (1)

$$F_z \equiv \rho_0 cos\phi \left\{ \left[f - (a cos\phi)^{-1} (\overline{u}cos\phi)_\phi \right] \frac{\overline{v'\theta'}}{\overline{\theta_z}} - \overline{w'u'} \right\}$$ (2)

$$\nabla \cdot \vec{F} \equiv -(\rho_0 \overline{u'v'})_\phi + \left(\rho_0 f \frac{\overline{v'\theta'}}{\overline{\theta_z}} \right)_z$$ (3)

where ρ_0 represents the density; z represents the altitude; a represents the radius of the Earth; ϕ represents the latitude; f represents the Coriolis parameter; θ represents the potential temperature; u and v represent the zonal and meridional winds, respectively; and w represents the vertical velocity. The overbars represent the zonal average, and the primes represent deviations with respect to the zonal average. We ignore the term $\overline{w'u'}$ because it is small relative to the other terms (Zhang et al., 2019; Zhao et al., 2022).

2.2.1.2 Refractive index

The quasigeostrophic refractive index (RI) is used to diagnose the environment of wave propagation (Chen and Robinson, 1992) and is calculated as:

$$RI = \frac{\overline{q_\varphi}}{\overline{u}} - \left(\frac{k}{a\cos\varphi} \right)^2 - \left(\frac{f}{2NH} \right)^2$$ (4)

where the meridional gradient of the zonal mean potential vorticity is calculated as:

$$\overline{q_\varphi} = \frac{2\Omega}{a}\cos\varphi - \frac{1}{a^2}[\frac{(\overline{u}\cos\varphi)_\varphi}{a\cos\varphi}]_\varphi - \frac{f^2}{\rho_0}(\rho_0 \frac{\overline{u_z}}{N^2})_z$$ (5)

where $-\frac{f^2}{\rho_0}\left(\rho_0 \frac{\overline{u_z}}{N^2} \right)_z = \left(\frac{f^2}{HN^2} + \frac{f^2}{N^4}\frac{dN^2}{dz} \right)\overline{u_z} - \frac{f^2}{N^2}\overline{u_{zz}}$, and $H, q, k, N^2, \Omega, u_z$ are the scale height, potential vorticity, zonal wavenumber, buoyancy frequency, Earth's angular frequency, and zonal wind shear, respectively. The refractive index squared could be affected not only by atmospheric stability and wind shear but also by the quadratic vertical shear of the zonal mean

zonal wind. As discussed in Matsuno (1970), it is expected that planetary waves of wavenumber k tend to propagate toward regions where $n_k^2 > 0$ and are inhibited in regions where $n_k^2 < 0$.

2.2.1.3 The Brewer-Dobson circulation

120 The Brewer-Dobson circulation (BDC) is driven by wave breaking in the stratosphere, and the BDC in the atmosphere is represented in log-pressure coordinates as follows (Andrews et al., 1987):

$$\overline{v}^* \equiv \overline{v} - \rho_0^{-1}(\rho_0 \overline{v'\theta'} / \overline{\theta}_z)_z \tag{6}$$

$$\overline{w}^* \equiv \overline{w} + (a\cos\phi)^{-1}(\cos\phi \cdot \overline{v'\theta'} / \overline{\theta}_z)_\phi \tag{7}$$

where $\overline{v}^*$ and $\overline{w}^*$ are the zonal-mean meridional and vertical velocities, respectively, θ is the potential temperature, a

125 is the radius of Earth, ϕ is the latitude, ρ_0 is the air density, and z is the log-pressure height.

Using the generalized downward control principle, the BDC can be further decomposed into different forcing terms (Song and Chun, 2016):

$$\overline{v}^* = -\frac{1}{\rho_0 \cos\varphi}\frac{\partial}{\partial z}\left\{-\cos\varphi\int_z^\infty \rho_0\left[\frac{\frac{1}{\rho_0 a\cos\varphi}\nabla\cdot\mathbf{F} + \overline{\mathrm{GWD}} + \overline{X} - \frac{\partial\overline{u}}{\partial t}}{f - \frac{1}{a\cos\varphi}\frac{\partial}{\partial\varphi}(\overline{u}\cos\varphi)}\right]dz'\right\} \tag{8}$$

130

$$\overline{w}^* = \frac{1}{\rho_0 a\cos\varphi}\frac{\partial}{\partial\varphi}\left\{-\cos\varphi[\int_z^\infty \rho_0[\frac{\frac{1}{\rho_0 a\cos\varphi}\nabla\cdot\mathbf{F} + \overline{\mathrm{GWD}} + \overline{X} - \frac{\partial\overline{u}}{\partial t}}{f - \frac{1}{a\cos\varphi}\frac{\partial}{\partial\varphi}(\overline{u}\cos\varphi)}]dz'\} \tag{9}$$

where $\nabla\cdot\mathbf{F}, \overline{\mathrm{GWD}}, \overline{X}$, and $\partial\overline{u}/\partial t$ represent the E-P flux divergence, gravity wave forcing, residual term of the transformed Eulerian mean (TEM) equations, and zonal-mean zonal wind tendency, respectively. Song and Chun (2016) reported that the gravity wave drag term $\overline{\mathrm{GWD}}$ and the residual term $\overline{X}$ are relatively smaller than the E-P flux divergence and zonal mean zonal wind tendency terms. Therefore, $\overline{\mathrm{GWD}}$ and $\overline{X}$ are not considered in this study.

135 ### 2.2.1.4 Takaya-Nakamura wave-activity flux

The Takaya-Nakamura (T-N) wave activity flux (Takaya and Nakamura 1997; 2001; Nakamura et al., 2010) is used to represent the three-dimensional energy dispersion characteristics of the quasistationary Rossby wave with respect to climatological mean flow:

$$W = \frac{pcos\phi}{2|U|} \cdot \left\{ \begin{array}{l} \frac{U}{a^2cos^2\phi}\left[\left(\frac{\partial\psi'}{\partial\lambda}\right)^2 - \psi'\frac{\partial^2\psi'}{\partial\lambda^2}\right] + \frac{V}{a^2cos\phi}\left[\frac{\partial\psi'}{\partial\lambda}\frac{\partial\psi'}{\partial\phi} - \psi'\frac{\partial^2\psi'}{\partial\lambda\partial\phi}\right] \\ \frac{U}{a^2cos\phi}\left[\frac{\partial\psi'}{\partial\lambda}\frac{\partial\psi'}{\partial\phi} - \psi'\frac{\partial^2\psi'}{\partial\lambda\partial\phi}\right] + \frac{V}{a^2}\left[\left(\frac{\partial\psi'}{\partial\phi}\right)^2 - \psi'\frac{\partial^2\psi'}{\partial\phi^2}\right] \\ \frac{f_0^2}{N^2}\left\{\frac{U}{acos\phi}\left[\frac{\partial\psi'}{\partial\lambda}\frac{\partial\psi'}{\partial z} - \psi'\frac{\partial^2\psi'}{\partial\lambda\partial z}\right] + \frac{V}{a}\left[\frac{\partial\psi'}{\partial\phi}\frac{\partial\psi'}{\partial z} - \psi'\frac{\partial^2\psi'}{\partial\phi\partial z}\right]\right\} \end{array} \right\} \tag{10}$$

where the superscript is the zonal deviation and where ϕ, λ, Φ, $f = 2\Omega\sin\phi$, a, Ω are the latitude, longitude, geopotential height, Coriolis parameter, earth radius and Earth rotation rate, respectively. $\psi' = \frac{\phi'}{f}$ represents the perturbation of the quasiground transfer function relative to the climate field, and $U = (U,V)$ represents the climatological basic flow fields.

2.2.1.5 Transformed Eulerian-Mean formulation

This study uses the Transformed Eulerian-Mean (TEM) formulation of the zonal-mean tracer continuity equation in log-pressure and spherical coordinates in order to accurately diagnose the eddy forcing of the zonal-mean transport of stratospheric ozone. BDC and eddy transports are calculated using terms (1) and (2), respectively (Monier and Weare 2011; Abalos et al. 2013; Zhang et al., 2017):

$$\frac{\partial\overline{\chi_{O_3}}}{\partial t} = \frac{\overline{v}^*}{R}\frac{\partial\overline{\chi_{O_3}}}{\partial\phi} - \overline{w}^*\frac{\partial\overline{\chi_{O_3}}}{\partial z}\,(term1)$$
$$-\frac{1}{\rho_0}\nabla\cdot M\,(term2) \tag{11}$$
$$+\overline{S}\,(term3)$$

where $\overline{S}$ is the sum of all chemical sources and sinks, $\overline{\chi}_{O_3}$ is the zonal-mean ozone concentration, $\overline{v}^*$ and $\overline{w}^*$ are the meridional and vertical BDC velocities (Andrews et al. 1987), respectively; M is the eddy flux vector, which is represented as:

$$\left[\rho_0\left(\overline{v'\chi_{O_3}'} - \frac{\overline{v'\theta'}}{\overline{\theta}_z}\frac{\partial\overline{\chi_{O_3}}}{\partial z}\right), \rho_0\left(\overline{w'\chi_{O_3}'} + \frac{1}{R}\frac{\overline{v'\theta'}}{\overline{\theta}_z}\frac{\partial\overline{\chi_{O_3}}}{\partial\phi}\right)\right], \tag{12}$$

$\nabla\cdot M$ is the divergence of the eddy flux vector and represents the eddy transport of ozone; ρ_0 is air density; θ is potential temperature; R is Earth's radius; t is time; ϕ and z are latitude and height, respectively.

In Eqs. (1)–(12), the overbar denotes zonal-mean quantities, and the prime indicates departure from the zonal mean. The subscripts denote partial derivatives. The Fourier decomposition is used to obtain components $u', v', and\ \theta'$ in Eqs. (1)–(3) and components $\nabla \cdot F\ and\ \psi'$ in (8)–(10) with different zonal wave numbers.

2.2.2 Statistical methods

160   The trend is measured by the slope of a linear regression based on least squares estimation. We use a two-tailed Student's t test to calculate the significance of the trend or perform a mean difference analysis. This paper measures the results of the significance test with p values or confidence intervals. $p \leq 0.1$ indicates that the trend or mean difference is significant at/above the 90% confidence level.

165   In this study, the normalized time series are standardized using Z-score standardization, where the data are processed using

the following formula: $A_{s-value} = \dfrac{A_{o-value} - \bar{A}}{\sigma_A}$, where $A_{s-value}$ denotes the normalized A-value, $A_{o-value}$ denotes original

A-value, $\bar{A}$ denotes average A-value, σ_A denotes standard deviation.

2.3 Model and experimental configurations

The F_1955-2005_WACCM_CN (F55WCN) component in the Community Earth System Model (CESM) Version 1.2.2 is
170   used. The F55WCN includes an active atmosphere and land, a data ocean (run as a prescribed component by simply reading sea surface temperature forcing data instead of running an ocean model) and sea ice. The model resolution is 1.9° latitude by 2.5° longitude, with 66 vertical levels and extending from surface to around 5.96×10^{-6} hPa. The chemistry module in F55WCN calculates the concentrations of different species and includes both gas phase and heterogeneous chemistry in stratosphere. The physics schemes in the F55WCN are based on those in the Community Atmosphere Model, Version 4
175   (CAM4; Neale et al., 2013).

To understand the causality of the ozone-circulation coupling, we perform model experiments to isolate the impact of ozone changes on stratospheric dynamics and circulation. Two groups of ensemble climate model experiments (i.e., the control experiment and O3clm experiment) use identical boundary conditions and initial conditions. Each group simulation consists
180   of 5 ensemble members, with initial temperature conditions randomly perturbed. Both of the two experiments run from 1970–2020, and the first 10 years are the spin-up time. The control experiment uses fully interactive ozone chemistry, and long-term stratospheric ozone changes are involved in the radiation scheme. In contrast, in the O3clm experiment, the climatological mean ozone is represented by monthly 3-dimensional mean data from a 1980-clim experiment, which is imported into the radiation scheme. In the 1980-clim experiment, surface emissions, external forcing, stratospheric aerosols, fixed lower
185   boundary conditions, and the solar photon enerspectra are all fixed at 1980. The 1980-clim experiment runs for 40 years with

the first 10 years as spin-up time and the remaining 30 years of data are used to drive the radiation scheme of the O3clm experiment. This results in the production of fixed radiative feedback, which is to say that the ozone-climate interactions over a long period are not radiatively active. Meantime, this setting is designed to preserve the seasonal temperature variations that conform to the background environmental conditions of the Earth and ensure stable operation of the experiment. Thus, the comparison between the ensemble mean of control and O3clm experiments isolates the feedback effects of long-term stratospheric ozone changes on atmospheric temperature and circulation from climate variability. Figure 1 (adapted from Friedel et al. 2022a, 2022b) provides the inspiration for the experimental design, which is crucial to understanding the analysis presented in this study.
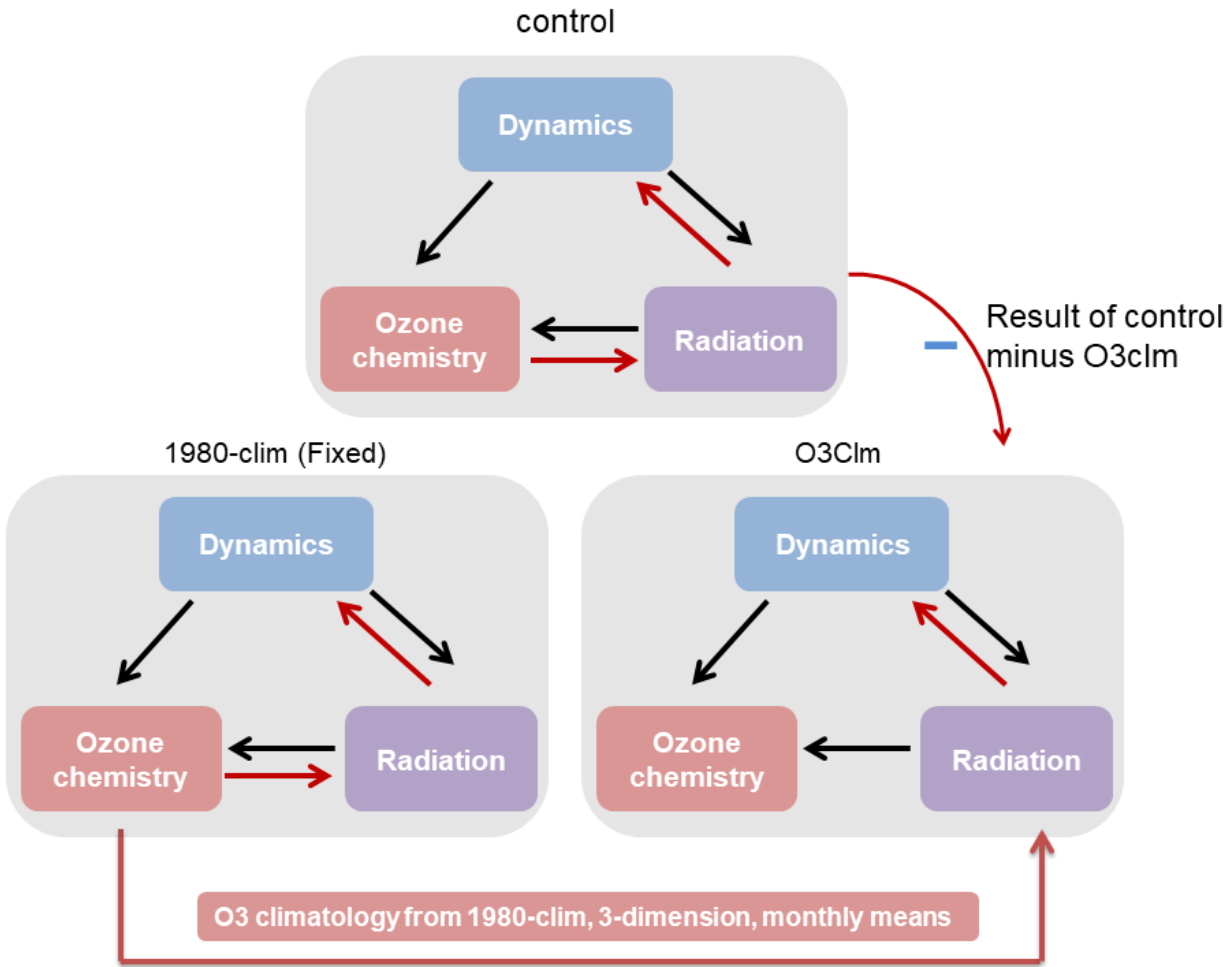
Figure 1 Simulation setup of the ensemble control and O3clm experiments. The control experiment treats ozone chemistry fully interactively. That is, the calculated ozone field has direct feedback on the atmosphere via the model radiation scheme. In contrast, the ensemble O3clm experiments do not use interactively calculated ozone in the radiation module. Instead, the radiation module uses an ozone climatology,

which is derived from the 1980-clim experiment (see Method text) (This figure adapted from Fig. 3a in Friedel et al., 2022a and Fig.1 in Friedel et al., 2022b).

3 Trends in temperature and ozone over the Arctic in the middle and lower stratosphere

In this study, we primarily focus on a detailed analysis in the pre-2000 period from 1980 to 2000, during which significant stratospheric ozone depletion occurred (LOTUS, 2019; IPCC, AR6, 2023). The changes after 2000 are briefly discussed. Figure 2 displays the normalized time series and linear trends in temperature in the Arctic stratosphere (over 65°–90°N), averaged between 10 and 150 hPa, during different periods from early winter to early spring. In November–December, the Arctic stratospheric temperature exhibits a small positive trend in the pre-2000 period in both the MERRA2 and ERA5 reanalysis datasets, and it shows an insignificant negative trend after 2000 (Fig. 2a; the black line represents MERRA2; the gray line represents ERA5). This suggests that there is a warming trend in the Arctic stratosphere during early winter in the pre-2000 period, followed by a cooling trend in the post-2000 period. The ensemble mean of control experiments reproduces these trends well, with a significant positive trend in temperature before 2000 and a significant negative trend after 2000 (Fig. 2a; purple line). From January to February, the temperature displays an insignificant negative trend before 2000 and a significant negative trend after 2000, derived from the three datasets (Fig. 2b). In March–April, the temperature shows a significant negative trend before 2000. After 2000, There is an unremarkable positive trend in MERRA2 and ERA5 datasets and an insignificant negative trend in ensemble mean of the control experiments (Fig. 2c). Overall, the long-term trends in temperature derived from the ensemble mean of control experiments are nearly consistent with the results from the reanalysis datasets, both in the period before 2000 and after 2000. The reasons responsible for the intra-seasonal opposite temperature trends are investigated in the following section.
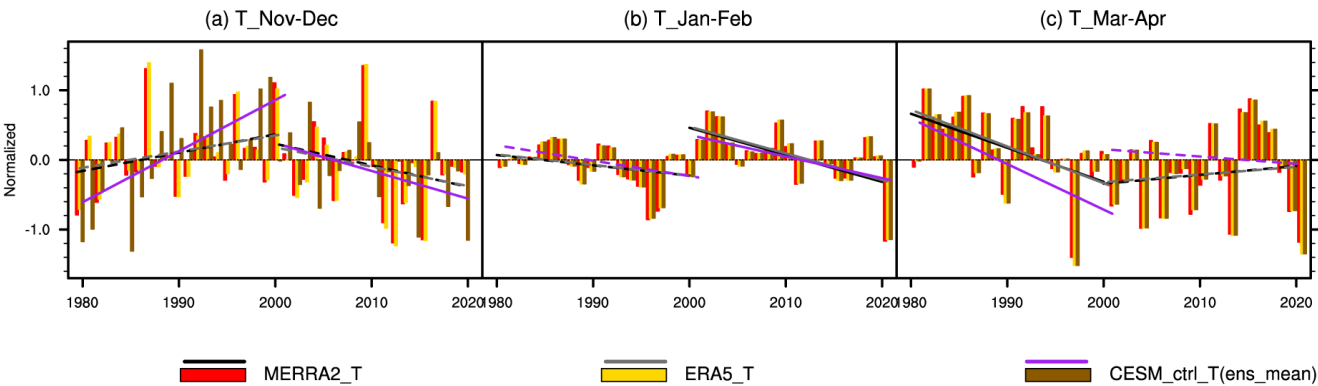
Figure 2 Normalized time series of the temperature averaged from 150 hPa to 10 hPa over 65°–90°N from 1980–2020 in (a) November–December, (b) January–February, and (c) March–April derived from MERRA2 (red column), ERA5 (orange column) and CESM ensemble mean of control experiments (brown column). The color straight lines represent the linear trends before 2000 and after 2000. Solid lines

indicate that the trends are statistically significant at the 90% confidence level according to Student's *t* test (for details of the normalization method, refer to Section 2.2.2: Statistical methods).

Figure 3 shows the trends in daily temperature and ozone between 10 and 250 hPa in the polar cap regions (65°–90°N) before
225 2000, which are based on data from MERRA2 and the ensemble mean of the control experiments. The trend reversal phenomenon is evident in December, which is consistent with Fig. 2. During November and December, there is an increasing trend in both temperature and ozone across all levels (Fig. 3a, b). While after December, the trends in temperature and ozone reverse in the middle stratosphere and then in the lower stratosphere. Similar trend patterns are found in the ensemble control experiments (Fig. 3c, d), indicating that the ensemble mean of the control experiments can reproduce the long-term trends in
230 stratospheric temperature and ozone in both early and late winter in the stratosphere. Therefore, it is reliable to use the CESM model to analyze these trends in the following text.
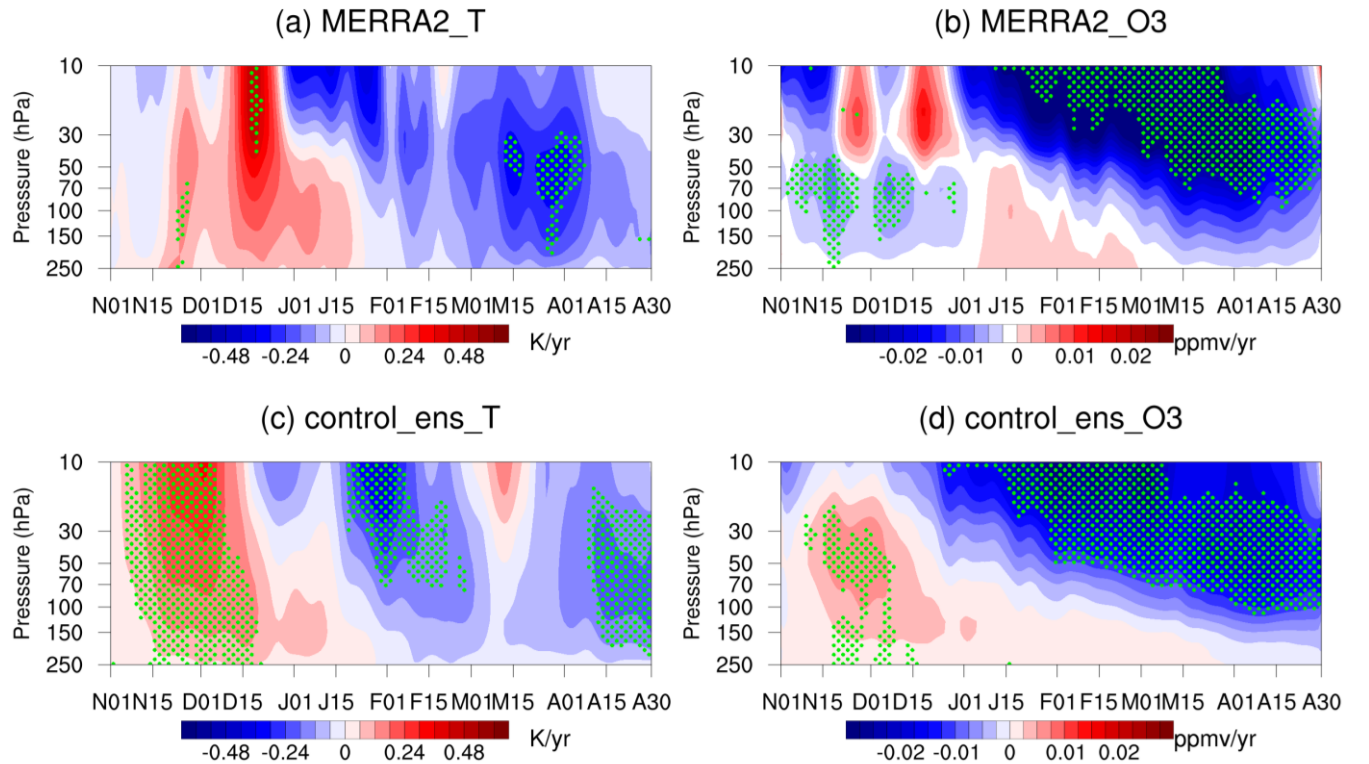
Figure 3 Time evolution of trends in daily (a, c) temperature and (b, d) ozone between 10 and 250 hPa in the polar cap regions (65°–90°N) during winter and spring derived from MERRA2 and the ensemble mean of control experiments in the pre-2000 period. The green dotted
235 regions indicate that the trends are statistically significant at the 90% confidence level according to Student's *t* test.

Figure 4a and b show the daily trends in temperature and ozone between 10 and 250 hPa in the polar cap regions (65°–90°N) before 2000 derived from the ensemble O3clm experiments (for the simulation set-up, see Methods). The ensemble mean of

O3clm experiments shows a nonsignificant temperature positive trend from November–December and a slightly unremarkable negative trend after December. This result is similar to that of the ensemble control experiments, but weaker and not significant (Fig. 3c). The stratospheric ozone exhibits marginally positive trends between 30 and 250 hPa in November and December, and shows a significant negative trend between 10 and 70 hPa after December, which is weaker than that in the ensemble control experiments. Given that the ensemble O3clm experiments excludes the radiative and dynamic feedback of long-term ozone changes, the stratospheric ozone decline in late winter and spring essentially reflects the ozone depletion induced by increasing ODSs in the pre-2000 period (Fig. 4b). And the temperature cooling in late winter and spring (Fig. 4a) may be related to stratospheric cooling induced by GHG (Tett et al., 1996; Hu and Guan, 2022). Fig.4c and 4d shows the differences in temperature and ozone trends before 2000 between the ensemble mean of the control experiments and O3clm experiments. Note that there are significant positive anomalies in temperature and ozone trends during November and early December, and significant negative anomalies after December, which are due to net ozone chemical-radiative-dynamical feedback effects (Fig. 4c, d). These significant differences suggest that ozone-climate interactions are crucial for long-term changes in Arctic stratospheric temperature and ozone.
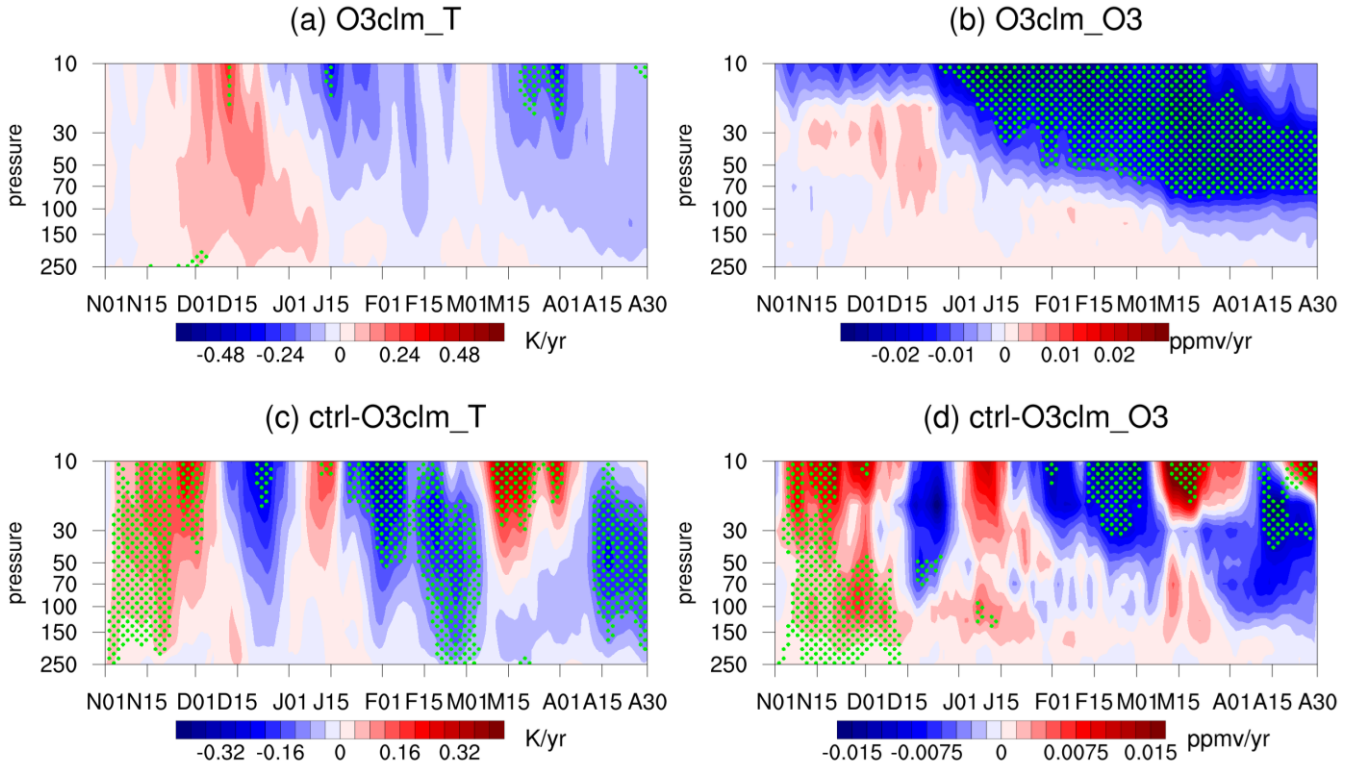
Figure 4 Time evolution of the trend of daily temperature and ozone over the levels between 10 and 250 hPa in the polar cap regions (65°–90°N) during winter and spring derived from (a–b) the ensemble mean of the O3clm experiments and (c–d) the differences between the ensemble control experiments and ensemble O3clm experiments before 2000. The green dotted regions indicate that the trend is statistically significant at the 90% confidence level according to Student's *t* test.

4 The factors responsible for the trends in temperature from winter to spring

The core process of ozone-climate interactions is ozone-circulation feedback. Figure 5 displays the trend in the vertical component downwelling branch of the BDC ($\overline{w}^*$) averaged over the polar regions (65°–90°N) during the pre-2000 period in both the ensemble control experiments and O3clm experiments. We also decomposed these trends into contributions from wave 1 (Fig. 5b, e and h) and wave 2 (Fig. 5c, f and i). The ensemble mean of control experiments shows significant negative trends in $\overline{w}^*$ from November to early December, corresponding to enhanced downwelling compared to climatological mean, and positive trends in $\overline{w}^*$ from late December to January, corresponding to weakened downwelling (Fig. 5a). In late February and early March, the $\overline{w}^*$ trend in the upper stratosphere becomes negative (Fig. 5a). The linear trends in $\overline{w}^*$ are basically opposite to those in temperature derived from the ensemble control experiments (Fig. 3c), which is because the enhanced downwelling (upwelling) favors polar adiabatic warming (cooling). Additionally, the $\overline{w}^*$ trend contributed by wave 1 is similar to the total trend, suggesting that wave 1 dominates the trends in $\overline{w}^*$. In the ensemble O3clm experiments, there is no negative trend in $\overline{w}^*$ in November and early December (Fig. 5d–f). This result indicates that ozone-circulation feedback strengthens the $\overline{w}^*$ in early winter, leading to adiabatic warming; conversely, there are anomalous upward motions that induce anomalous adiabatic cooling from January to February, which is consistent with the reversal of the temperature trend in January (Figs. 3, 4). The differences between the ensemble mean of the control experiments and O3clm experiments suggest a similar pattern to that of the ensemble control experiments (Fig. 5g, h and i). Overall, the changes in the $\overline{w}^*$ during early winter, particularly in November are, mainly modulated by the ozone-climate interactions, and adiabatic warming due to the strengthening of the $\overline{w}^*$ plays a crucial role in Arctic temperature from November to early December. Similar results have been reported in previous studies (Albers and Nathan, 2013; Hu, et al., 2019b).
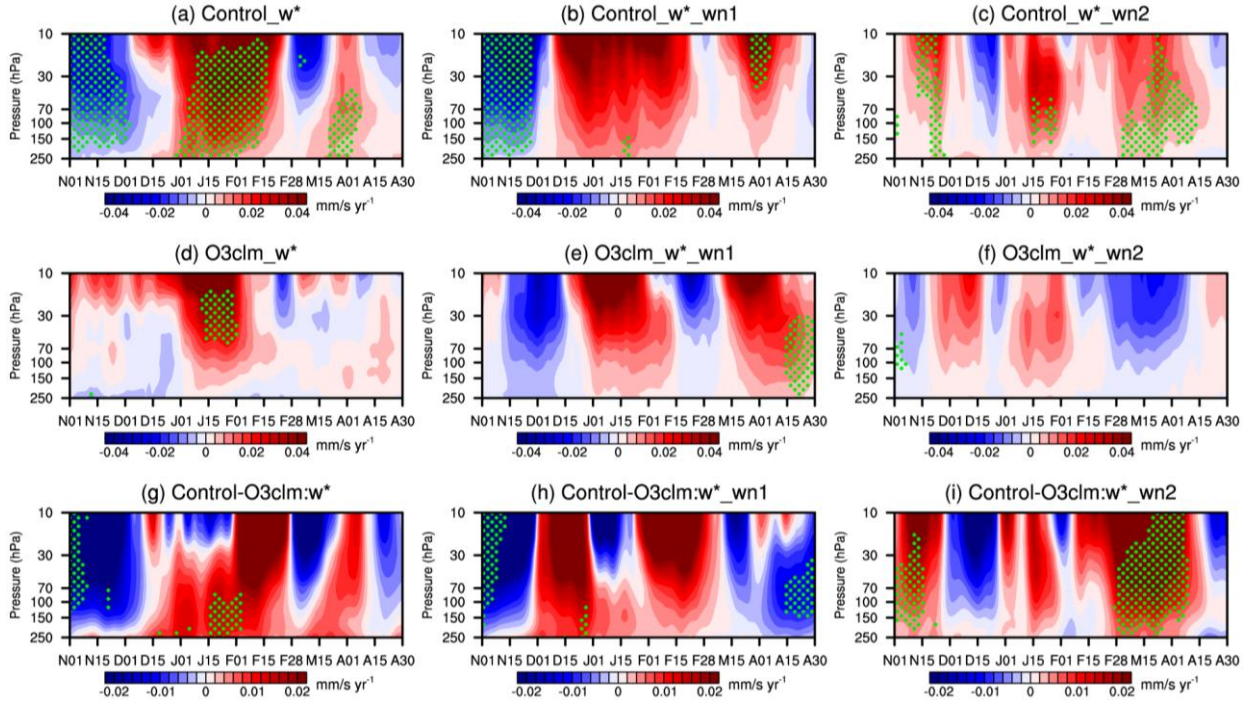
Figure 5 Linear trend of (a, d, and g) the vertical component of the BDC ($\overline{w}^*$) and its contribution (shading) from (b, e and h) the wavenumber 1 and (c, f and i) wavenumber 2 components before 2000 between 10 and 250 hPa averaged in the polar regions (65°–90°N) during winter and spring, derived from (a, b and c) the ensemble control experiments, (d, e and f) ensemble O3clm experiments and (g, h and i) the differences between the ensemble control experiments and ensemble O3clm experiments. The green stippled regions indicate the trend of the BDC significant at the 90% confidence level according to Student's *t* test (The daily data are first processed with a 30-day low-pass filter to remove high-frequency signals).

Furthermore, the enhanced BDC may have an effect on the ozone concentration. The increase in stratospheric ozone during November–December and decrease during January–February (Fig. 4d) induced by ozone-circulation feedback is caused by enhanced dynamical transport. We focus on the role of the BDC in driving the ozone increase in early-winter and its decrease in mid-winter, investigating the reasons for the reversal. Figure 6 shows the trend in stratospheric ozone budget from November to February between 10 and 250 hPa in the polar regions (65°–90°N) in the pre-2000 period, which is decomposed into BDC and eddy transport of ozone (calculated by Eqs. (11), (12)). In the ensemble control experiments, from November to December (early winter), the total ozone budget shows a significantly positive trend, indicating an increase in ozone concentrations. This trend is primarily driven by the sum of BDC and eddy transport. In mid-winter, the trend in ozone budget weakens and changes to negative, indicating a leveling off of increased ozone concentration. In contrast, in the ensemble O3clm experiments, the trend in the ozone budget is opposite to those in the ensemble control experiments and is not statistically significant from

295 November to February. This demonstrates that during early winter, the accelerated BDC intensifies poleward ozone advection through directly transports ozone-rich air masses from tropical reservoirs to polar region, and enhances downward transport of ozone from the upper stratosphere to lower stratosphere. The transport of ozone due to ozone-circulation feedback is reconfirmed by the difference between the ensemble mean of the control and O3clm experiments. In January, the difference between the two experiments shows an intra-seasonal reverse in ozone transport, indicating that the ozone-circulation
300 interactions can also give feedback to ozone concentrations.
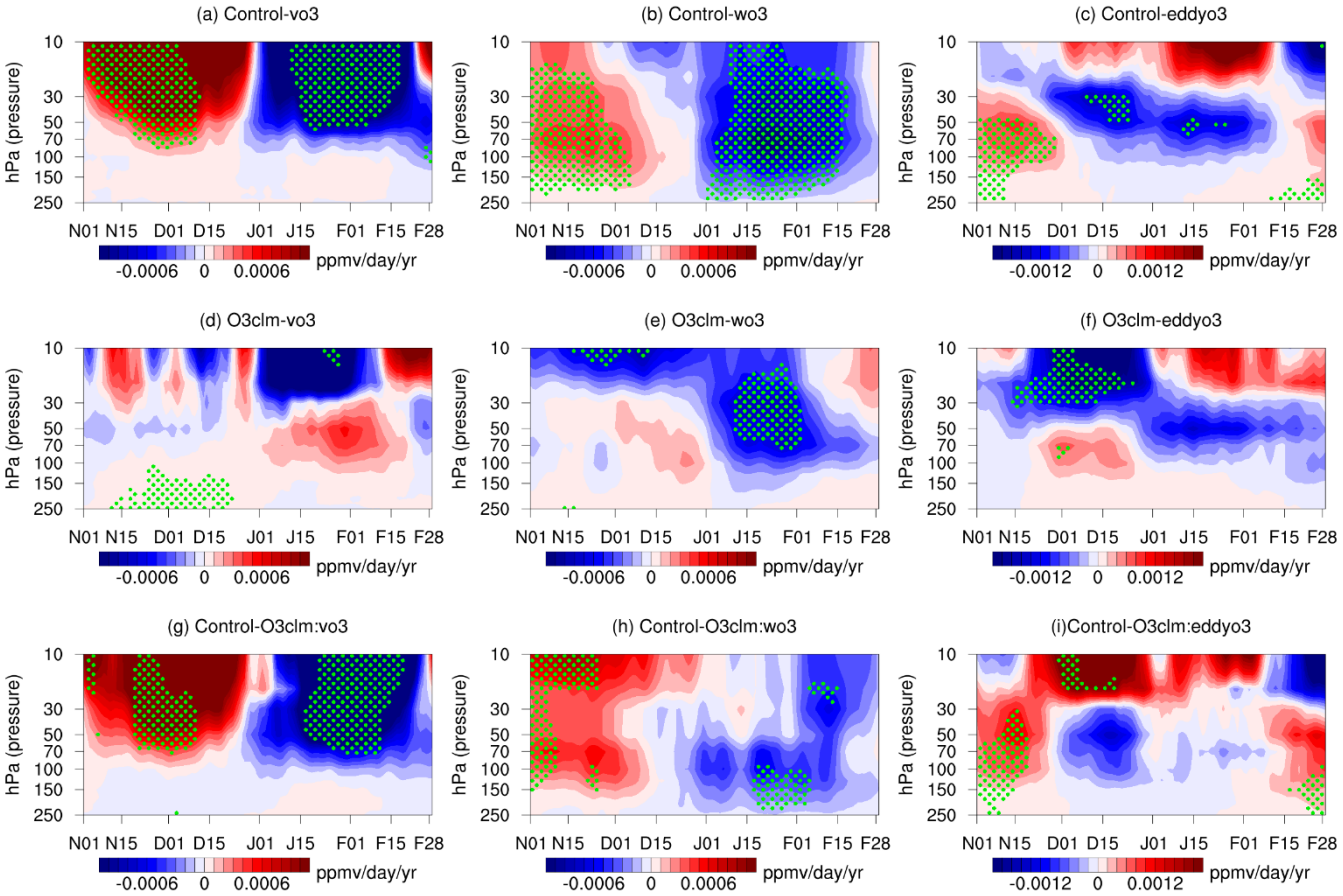
Figure 6 Dynamically produced ozone concentration trend, decomposed into (a, d and g) meridional and (b, e and h) vertical BDC transport and (c, f and i) eddy transport between 10–150 hPa in the polar regions (65°–90°N) from November to February, derived from (a–c) the ensemble control, (d–f) the O3clm experiments and (g–i) the difference between the two experiments during the pre-2000 period. The trend
305 over the dotted regions is statistically significant at the 90% confidence level according to the Student's t test (The daily data are first processed with a 30-day low-pass filter to remove high-frequency signals). It is noted that the x-axes denoted the daily trend evolution from 1 November to 28 February.

BDC trends associated with ozone-climate interactions can be attributed to the upward planetary waves. Figure 7 shows the trends in stratospheric planetary wave activity over the subpolar regions (50°–80°N) from November to April. In the ensemble control experiments, there is a significantly positive trend in the waves entering the stratosphere in November and early December before 2000, which is accompanied by intensified wave flux convergence in the middle stratosphere (approximately 10–50 hPa; Fig. 7a). However, in late-December and January, the waves entering the stratosphere decrease, accompanied by weakened wave flux convergence. These features imply that stratospheric planetary wave activity strengthened in November and early December and weakened in late December and January during the pre-2000 period, which is consistent with the findings of previous studies (Bohlinger et al., 2014; Young et al., 2012). In contrast, in the ensemble O3clm experiments, waves entering the stratosphere in November and early December decrease, and there is no significant convergence trend before 2000 (Fig. 7d). The trends in the planetary wave are mainly contributed by the wave 1 component rather than by wave 2 (Fig. 7b, c, h and i). In November and early December, more propagation of planetary into the stratosphere weakens the circumpolar westerlies and increases the temperature in the Arctic lower stratosphere, which is consistent with the enhanced downward motions shown in Fig. 5g. The trends in planetary wave activity and E-P flux convergence in January and February are opposite to those in early winter. Overall, the changes in upward wave propagation and BDC make a major contribution to reverse the stratospheric temperature trend at the intra-seasonal timescale during winter. It is worth noting that the planetary wave activity only changes noticeably before February in the ensemble mean of control experiments and O3clm experiments, and then gradually weakens in spring. This suggests that dynamic feedback processes induced by ozone-climate interactions mainly occur in winter.
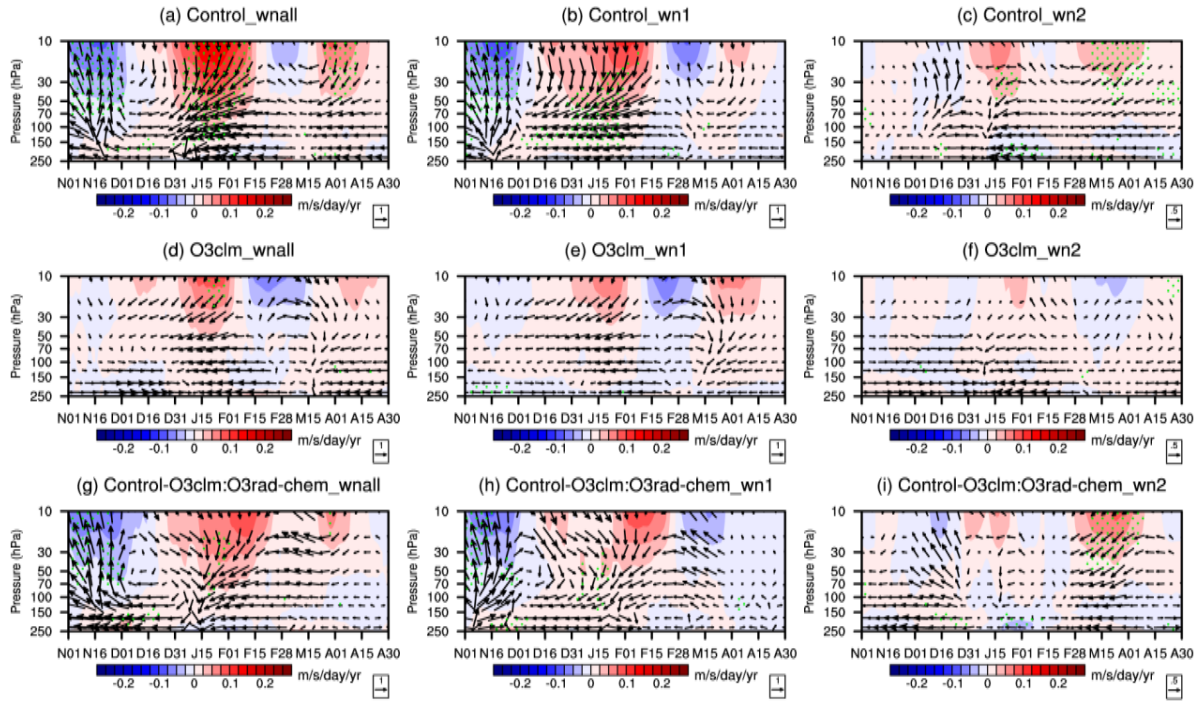
Figure 7 Trends in E-P flux (a, d and g; arrows; units of horizontal and vertical components are 10^4 and 10^2 kg s^{-2} yr^{-1}, respectively; an arrow pointing to the right indicates poleward propagation, whereas an arrow pointing to the left indicates equatorward propagation) and its divergence (shading) with their (b, e and h) wave 1 components and (c, f and i) wave 2 components over the levels between 10 and 250 hPa before 2000 averaged in the subpolar regions (50°–80°N) during winter and spring, as derived from (a–c) the ensemble control experiments, (d–f) ensemble O3clm experiments and (g–i) the differences between the ensemble control experiments and O3clm experiments. The green stippled regions indicate the trend of the E-P flux divergence significant at the 90% confidence level according to Student's *t* test (The daily data are first processed with a 30-day low-pass filter to remove high-frequency signals).

Previous studies emphasized that planetary waves entering the stratosphere are primarily modulated by propagating conditions in the upper troposphere and lower stratosphere regions (Albers and Nathan, 2013; Hu, et al., 2019b). The refractive index (RI) is a good metric for assessing the atmospheric state for planetary wave propagation. Theoretically, regions with a larger RI are more favorable for planetary wave propagation (Andrews et al., 1987). On the basis of the formula of the RI (see Eqs. (4) in the Methods section), the second term of the RI is a constant with specific wavenumbers, and the third term of the RI is negligible compared to the changes in the first term (Simpson et al., 2009; Hu, et al., 2019b; Hu, et al., 2022). It is suggested that variations in the meridional gradient of zonal mean potential vorticity ($\overline{q}_\varphi$) could account for most of the changes in the RI at mid- and high- latitudes (Simpson et al., 2009; Zhang et al., 2020). Figure 8 shows the daily evolution of the trend in the RI, the vertical component of the E-P flux (F_z) and $\overline{q}_\varphi$ averaged between 45°–75°N and U60 (zonal wind at 60°N) in the lower stratosphere (between 50–150 hPa) from November to February before 2000. The datasets are derived from the ensemble

control experiments and O3clm experiments. In the ensemble control experiments, significant positive trends in the RI persist during November in the middle and lower stratosphere (black line), implying that more planetary waves could enter the stratosphere due to ozone-climate interactions in early winter. This corresponds to the strengthened F_z (purple line in Fig.

350 8a and Fig. 7a). Higher $\overline{q}_\varphi$ values (blue line) lead to a larger RI, providing favorable atmospheric conditions for upward wave propagation. Note that the positive trends in $\overline{q}_\varphi$ and RI lead the increasing F_z by about week. However, after mid-December, the RI trends become negative in the middle and lower stratosphere, suppressing upward wave propagation, which is consistent with the reduced E-P flux during this period (Figs. 7a, 8a). There is a remarkable reversal of $\overline{q}_\varphi$ as a precursor. The reversal of the PV gradient ($\overline{q}_\varphi$) is primarily driven by changes in the zonal wind vertical shear term (U_{zz} term; not shown).

355 The negative $\overline{q}_\varphi$ trend persists until February in the middle and lower stratosphere, which basically corresponds to a negative trend in the RI, which consequently affects the intra-seasonal reversal signal in the E-P flux (Figs. 7a, 8a). Therefore, changes in $\overline{q}_\varphi$ could serve as a main factor influencing the changes in the RI, consequently impacting the propagation of planetary waves. However, in the ensemble O3clm experiments, for most of winter, the RI and F_z show insignificant negative trends, which are markedly different from those derived from the ensemble control experiments. Overall, the results indicate the

360 impact of ozone-climate interactions resulting from ozone depletion on wave propagation conditions through influencing $\overline{q}_\varphi$ and the RI.

Nathan and Cordero (2007) pointed that wave-induced ozone heating decrease wave drag by about 25% in the lower stratosphere, favoring planetary wave propagation at this altitude during early winter in the present study (Fig. 7a, g).

365 Additionally, they pointed out that photochemically accelerated cooling due to ozone augments the Newtonian cooling and increases the wave drag by a factor of two in the upper stratosphere, which is in accordance with our finding that ozone-climate interactions enhance the upper stratospheric E-P flux convergence (Fig. 7a, g). These analysis results highlight how ozone-climate interactions affect stratospheric dynamics processes. Specifically, in the ensemble control experiments, positive zonal wind vertical shear anomalies (not shown) at middle-latitudes in November increase the $\overline{q}_\varphi$, which in turn raises the RI and

370 enhances the F_z. The increase in planetary waves in early winter weakens the polar vortex compared to that in the O3clm experiment, leading to deceleration in circumpolar westerlies during mid-December and January (red lines in Fig. 8). The decreased zonal wind at 60°N further suppresses the vertical propagation of planetary wave in the subsequent winter months, corresponding to the intra-seasonal reversal of F_z before and after January. Then, the weakening of F_z in the ensemble control experiments allows for a stronger recovery of the polar vortex due to wave-flow interaction in February compared to

375 the O3clm experiments (red lines in Fig. 8). This intra-seasonal reversal of F_z explains the reversals of BDC and temperature around December (Figs. 3, 5), and this feature disappears in the ensemble O3clm experiments in which the ozone-interactions

are cut off, highlighting the key role of ozone-climate interactions in modulating stratospheric dynamics processes. It is worth noting that the stronger polar vortex during late winter in control experiments than O3clm experiments is also related to the radiative cooling, which will be discussed in Figure 11.

380
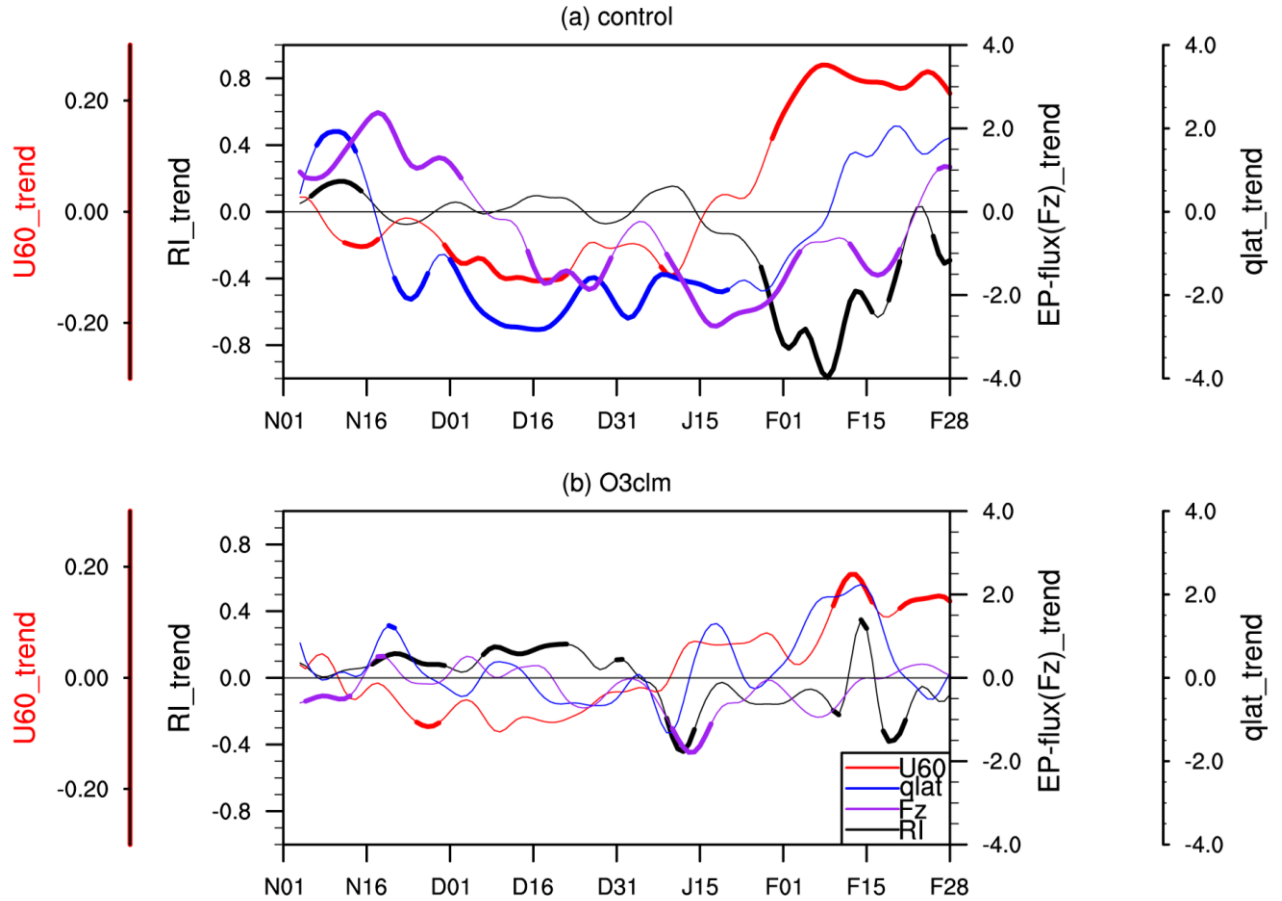
Figure 8 Daily evolution of the trends in the RI (black lines), vertical component of the E-P flux (F_z; purple lines), $\overline{q}_\varphi$ (blue lines), U60 (zonal wind at 60°N; red lines) before 2000 at 50–150 hPa averaged in mid-latitude (45°–75° N) from 1 November to 28 February, derived from (a) the ensemble mean of the control experiments and (b) O3clm experiments. The solid lines indicate the trends in the significant RI, vertical component of the E-P flux and $\overline{q}_\varphi$ at the 90% confidence level according to Student's t test (The daily data are first processed with a 7-day low-pass filter to remove high-frequency signals).

385

Figure 9 shows the trends in the zonal wavenumber 1 geopotential height and its climatology from November to January, as well as the difference in the T-N wave activity flux between the high-ozone (1980–1985) and low-ozone (1997–2002) periods. In the ensemble control experiments, the climatological mean displays a westward-tilted structure with increasing height. In

390 November, the zonal wavenumber 1 geopotential height tendency is somewhat in phase with the climatological mean,

indicating an amplification of wavenumber 1 baroclinic waves, particularly in the lower stratosphere. Furthermore, the T-N wave flux propagates upward to the eastern hemisphere, causing the wave center of the geopotential height to move eastward. In December, the positive center of the geopotential height anomalies shifts from 90°W to 0°, and the negative center shifts from 90°E to 180°, indicating that the geopotential height anomalies have shifted eastward by approximately 90° compared with those in November. As a result, the geopotential height anomalies are out of phase with the climatological mean, corresponding to weakened upward wave propagation in December. Note that there remains enhanced eastward wave propagation in the eastern hemisphere in the upper stratosphere during this month, leading to a further 60° eastward shift in geopotential height anomalies and a continuous weakening of stratospheric planetary wavenumber 1 in January. Correspondingly, an intra-seasonal reversal signal in the E-P flux is found in the ensemble mean of the control experiments (Fig. 7).
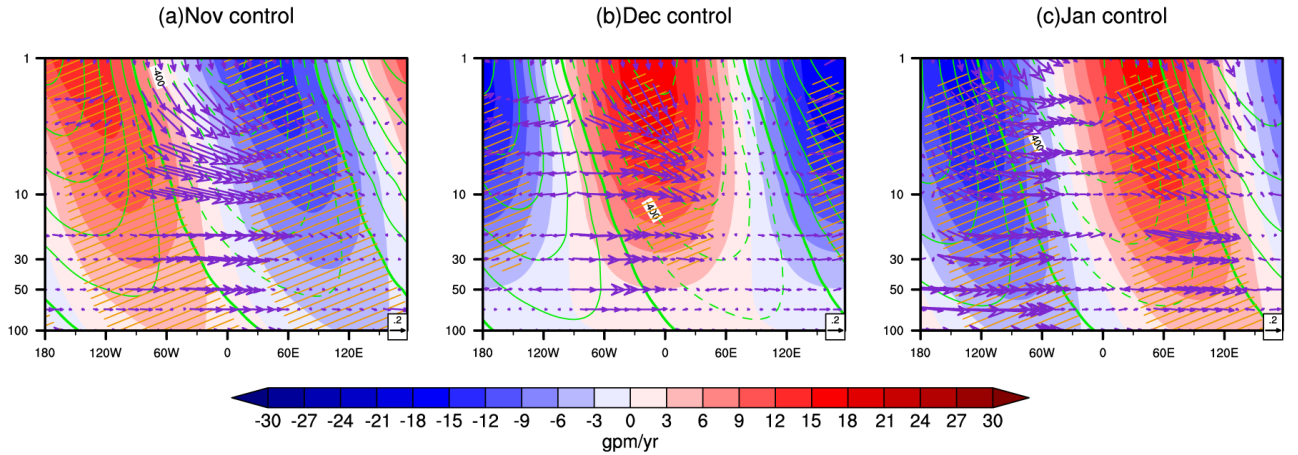
Figure 9 Height-longitude cross sections along 60°N of the zonal wave-1 geopotential height trend before 2000 (shaded areas) and the difference in T-N flux between the low-ozone period (1980–1985) and high-ozone period (1997–2002) (vector arrows) derived from the ensemble control experiments. The green contours indicate the climatological mean of the zonal wave-1 geopotential height derived from the ensemble mean of the control experiments. The orange lines represent values that are statistically significant at the 90% confidence level according to Student's *t* test.

In addition, the propagation of planetary wavenumber 1 can drive the Arctic stratospheric polar vortex toward Eurasia and promote polar vortex shift events (Mitchell et al., 2011; Zhang et al., 2016; Huang et al., 2018). The impacts of ozone-climate interactions on the position of the Arctic stratospheric polar vortex remain unclear. Figure 10 shows the potential vorticity (PV) differences and stratospheric polar vortex edge between the low- and high-ozone periods, derived from the ensemble control and O3clm experiments. In the ensemble control experiments, there are positive PV anomalies in eastern Eurasia during November and December in the low-ozone period, along with a shift in the position of the polar vortex edge toward eastern Eurasia. In contrast, in the ensemble O3clm experiments, the polar vortex edge shows no significant shift during the low-ozone period compare to that during the high-ozone period, and there are no significant changes in the PV anomaly in eastern Eurasia.

These findings further indicate that the ozone-climate interactions could amplify planetary wavenumber 1 (as shown in Figs. 7, 9), thereby influencing the shift in the polar vortex during early winter. The results indicate that the dynamic feedback of ozone-climate interactions significant influences on the position of the polar vortex in early winter. In addition, the positive PV anomalies over the eastern Eurasia induced by the polar vortex shift are consistent with the increased mid-latitude $\bar{q}_\varphi$

420 (Fig. 8a) and the enhanced stratospheric planetary wave activity in November (Figs. 7, 8), which reconfirms that the ozone-climate interactions can modulate stratospheric wave-mean flow interaction in early winter, which is consistent with the findings of Zhang et al. (2020).
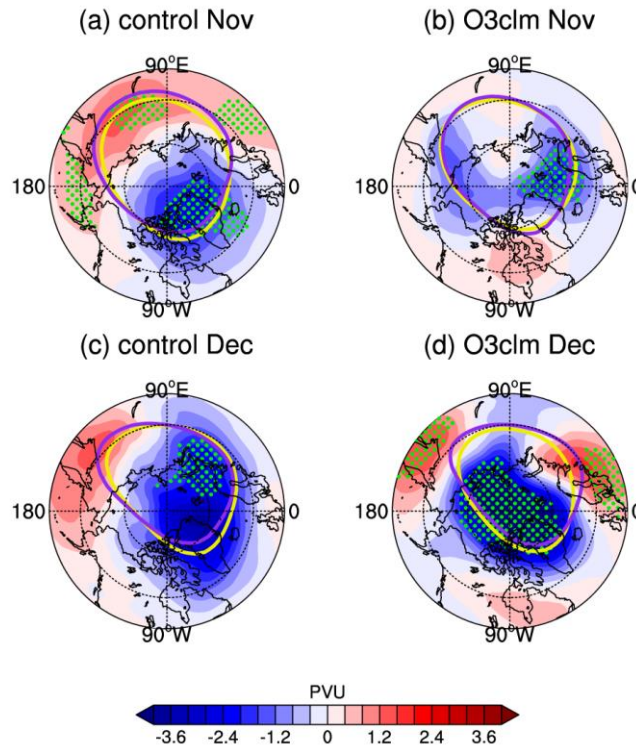
Figure 10 Differences in PV between the low-ozone period (1997–2002) and high-ozone period (1980–1985) averaged between 430 and
425 600 K (shaded) in (a, b) November and (c, d) December derived from (a, c) the ensemble control experiments and (b, d) O3clm experiments. The edges of the polar vortex in the low-ozone period and high-ozone period are represented by purple lines and yellow lines, respectively.

It is then natural to ask why there are distinct temperature responses in Arctic winter, in the absence of solar radiation, between the two experiments with and without ozone-climate interactions. Figure 11 shows the evolution of shortwave heating rate
430 (referred to as the QRS) and longwave heating rate (referred to as the QRL) from November to April in the two experiments. Both the ensemble control and O3clm experiments reveal relatively weak QRS trends from November to mid-February because sunlight cannot reach the Arctic regions. From the ensemble mean of the control experiments, the QRL heating from November to early December shows a negative trend corresponding to the longwave cooling effect (Seppälä et al., 2025). In contrast, in

the ensemble O3clm experiments, the ozone-climate interactions are removed and there are weaker QRL trends, which may

435 be solely contributed by GHGs. The QRL cooling in the ensemble control experiments occurs because a warmer air parcel corresponding to the positive temperature trend in early winter emits more longwave radiation and hence cools faster. Lin and Ming (2021) noted that radiative damping due to longwave cooling could intensify wave dissipation and further enhance subsidence of the BDC. Unlike their work, which focused on the ozone-circulation feedback processes in the Antarctic stratosphere, the present study offers more details on these processes in the Arctic winter stratosphere.

440

After February, the upward propagation of planetary waves and ozone-circulation feedback processes weaken, whereas the contribution of shortwave radiative processes to stratospheric temperature increases as sunlight reaches the Arctic region. The ensemble control experiments demonstrate that the QRS shows a significant negative trend during the ozone-depletion period, which leads to a lower temperature and an strengthened polar vortex (Brasseur and Solomon, 2005). However, in the ensemble

445 O3clm experiments, the radiative effects of ozone-climate interactions are inactivated, leading to insignificant changes in QRS throughout the entire winter and spring. In addition, negative temperature anomalies (Fig. 2c and Fig. 3a, c) correspond to the colder air parcel emitting less longwave radiation and causing warming to generate positive QRL anomalies in spring. In the differences between the ensemble control experiments and O3clm experiments, QRS and QRL exhibit similar patterns as those in the ensemble control experiments. Our results demonstrate that the ozone-climate interactions during early winter, mainly

450 influence stratospheric temperature through dynamic adjustments. In contrast, the trends in temperature during late winter and spring are primarily due to dynamic cooling and shortwave cooling overwhelming the longwave heating of radiation processes.
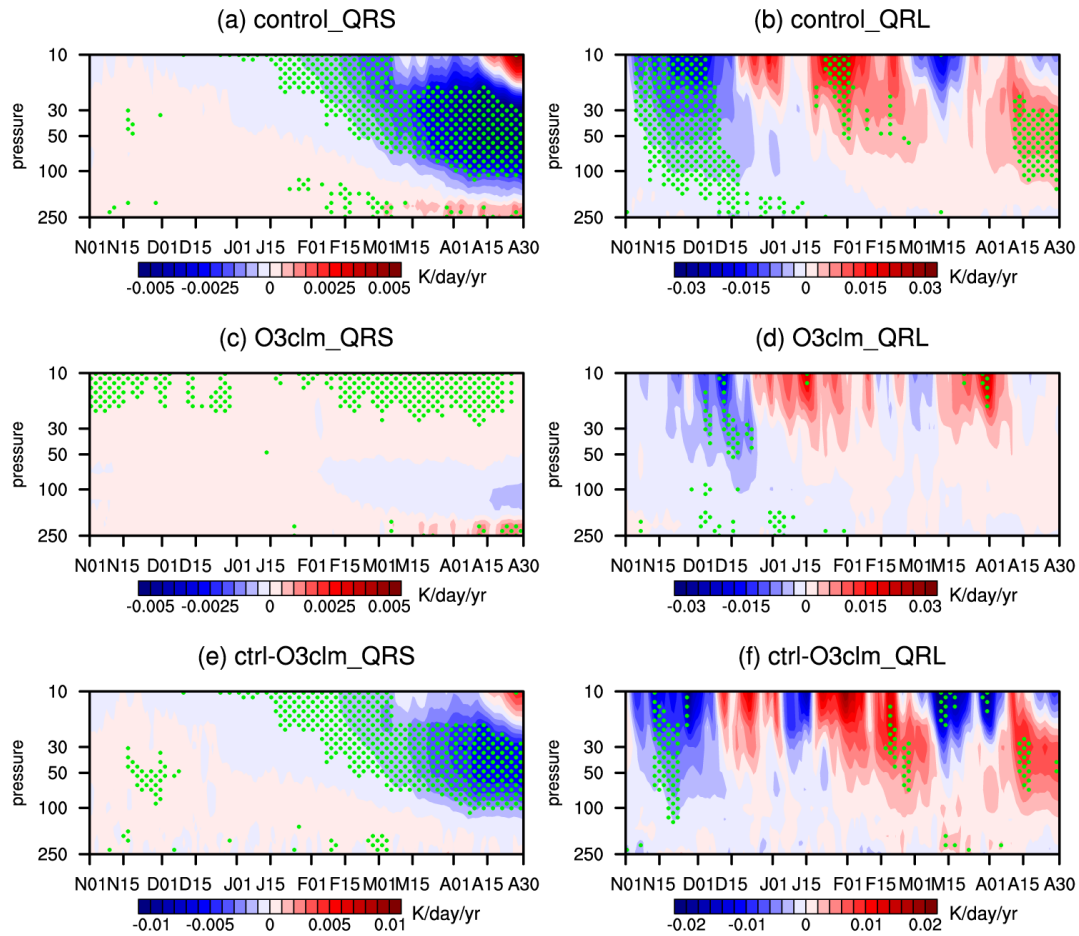
Figure 11 Time evolution of trends in the daily shortwave heating rate (solar heating rate; QRS) and longwave heating rate (QRL) between 10 and 250 hPa in the polar regions (65°–90°N) during winter and spring derived from (a, b) the ensemble control experiments, (c, d) ensemble O3clm experiments and (e, f) the differences between the ensemble mean of the two experiments before 2000. The green dotted regions indicate that the trends are statistically significant at the 90% confidence level according to Student's *t* test.

In the previous sections, we revealed the impact of ozone-climate interactions on stratospheric temperature and circulation during the ozone-depletion period before 2000. To understand how ozone-climate interactions work after 2000, Figure 12 further illustrates the trend in the daily variation in ozone and temperature between 10 and 250 hPa in the polar cap regions (65°–90°N) in the post-2000 period, on the basis of MERRA2 data. The results show an unremarkable decrease in ozone and temperature trends between 10 and 150 hPa during November. However, in December, there is a significant increasing trend in ozone across all levels and a slightly positive trend in temperature (Fig. 12a, b). From February to March, the temperature and ozone in the regions of the middle and lower stratosphere show significant negative trends. These changes are similar to those before 2000, with the difference being that the reversal of the negative trend occurs earlier, in late December. Compared

with the pre-2000 period, there are positive anomalies for temperature and ozone in the middle and upper stratosphere in April after 2000, indicating that the post-2000 period experienced stratospheric ozone recovery (WMO, 2022).

Figure 13 shows the results derived from the ensemble control experiments and ensemble O3clm experiments, and the
470   difference between the ensemble mean of the two experiments. The ensemble mean of control experiments shows an insignificant positive temperature in the lower stratosphere during November and December and negative temperature trends during January and February, which is similar to the MERRA-2 results. In the ensemble O3clm experiments, the temperature and ozone trends show totally different patterns with those in observation and the ensemble control experiments. Furthermore, in the post-2000 period, the stratospheric ozone shows significant positive trends in the O3clm experiments, which is not seen
475   in the observation and control experiments. This is because the negative ozone trends in March and April induced by ozone-climate interactions may delay ozone recovery during spring through the shortwave radiative cooling effect. Also note that the differences in temperature and ozone between the ensemble mean of the control experiments and O3clm experiments (Fig. 13e, f) look somewhat like the pre-2000 results (Fig. 4c, d), but the differences are not significant most of the time. This suggests that the ozone-climate interactions continue to work after 2000, leading to intra-seasonal reversal trends in
480   stratospheric temperature and ozone.
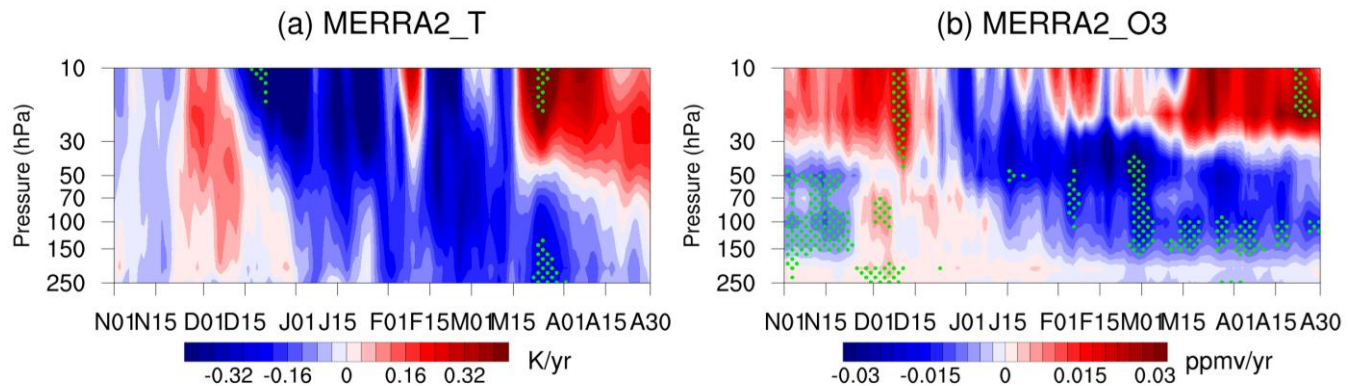
Figure 12 Time evolution of trends in daily (a) temperature and (b) ozone over the levels between 10 and 250 hPa in the polar cap regions (65°–90°N) during winter and spring derived from MERRA2 after 2000. The green dotted regions denote that the trends are statistically significant at the 90% confidence level according to Student's *t* test.
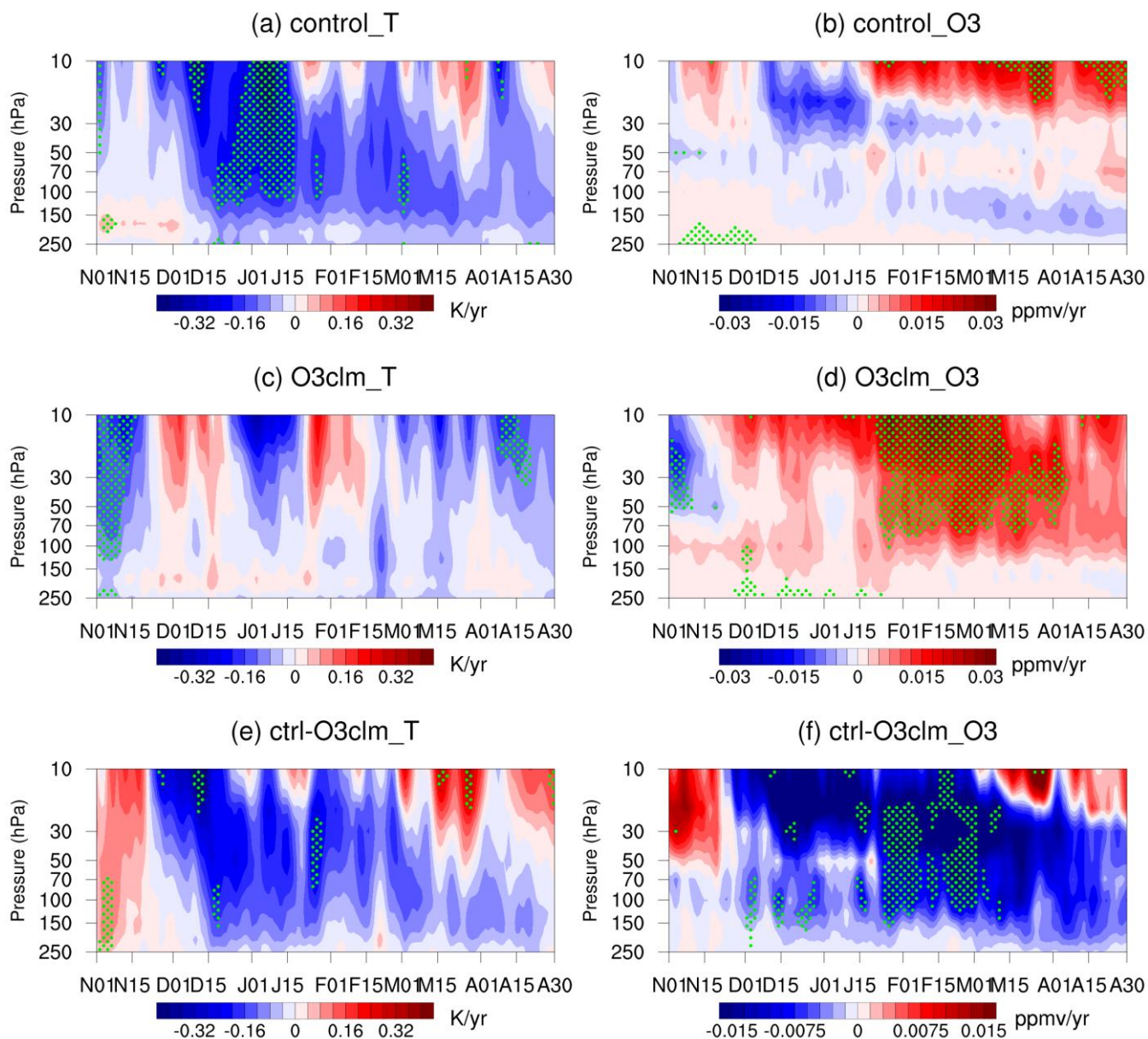
Figure 13 Time evolution of the trends in daily (a, c and e) temperature and (b, d and f) ozone over the levels between 10 and 250 hPa in the polar cap regions (65°–90°N) during winter and spring derived from (a, b) the ensemble control experiments, (c, d) the ensemble O3clm experiments and (e, f) the differences between the ensemble mean of the control experiments and O3clm experiments after 2000. The green dotted regions indicate that the trends are statistically significant at the 90% confidence level according to Student's *t* test.

5 Conclusion and discussion

This study investigates the impacts of ozone-climate interactions on the temperature trends in the Arctic stratosphere during winter and early spring, using reanalysis datasets and CESM model simulations. We found that stratospheric Arctic temperature in early winter particularly in November significantly increases before 2000 (Figs. 2, 3 and 4), which is primarily driven by enhanced planetary wave propagation into the stratosphere and a strengthened BDC. The enhanced BDC also increases the stratospheric ozone during early winter. Notably, the ozone-circulation feedback of ozone-climate interactions plays a key role in modulating this trend. Specifically, in early winter, ozone-circulation feedback can create an atmospheric state favorable for upward wave propagation, which is induced by the increases of $\overline{q}_\varphi$ in mid-latitude, and E-P flux convergence (Figs. 7, 8), which could lead to a strengthened BDC (Fig. 5) and thereby a positive trend in temperature and ozone (Figs. 3 and 6) during early winter. These trends in the BDC and planetary wave activity are predominantly driven by planetary wavenumber 1 (Figs. 5, 7). The wave-induced ozone heating increases lower-stratospheric wave propagation (Fig. 7, 8), and subsequently weakens the polar vortex during mid-winter (Fig. 10), accompanied with the decelerated circumpolar westerlies (Fig. 8). Then, the upward propagation of planetary waves is suppressed, and consequently, the Arctic stratospheric temperature show opposite trends in January and February to early winter. Additionally, the ozone-circulation feedback causes the T-N wave activity to propagate eastward and upward, resulting in the enhancement and eastward shift of the planetary wavenumber 1 (Fig. 9). This feedback causes the polar vortex to shift toward the eastern Eurasia continent (Fig. 10). During early spring, when solar radiation reaches the polar regions, reduction in ozone shortwave heating during the ozone-depletion period causesin the negative trends during spring (Fig. 11). After 2000, the stratospheric temperature response to ozone changes is weaker than that before 2000 (Figs. 12, 13).

The ozone-climate interactions are crucial processes in modulating above-mentioned Arctic stratospheric temperature trends. Similar to earlier findings, our study highlights the role of planetary wave activity and BDC in influencing Arctic stratospheric temperature. The present study provides more detailed information on the ozone-circulation feedback processes driven by ozone-climate interactions. The ozone-circulation feedback of interest are primarily the interactions between ozone changes, wave propagation, and BDC, which regulate the dynamics of the Arctic stratosphere. Ozone-induced changes in wave propagation could modulate the vertical motions in the Arctic lower stratosphere, leading to changes in stratospheric temperature and circulation. The ozone transport associated with circulation changes could give feedback effect on polar ozone redistribution. Notably, various factors may influence the ozone-climate interactions. These factors include changes in GHG concentrations, nitrous oxide, volcanic activity, or other atmospheric constituents that influence radiative and chemical processes in the stratosphere (Eric Klobas et al., 2017; Meul et al., 2016; Ravishankara et al., 2009; Revell et al., 2015; Solomon et al., 2009). This raises questions about other potential feedback mechanisms for ozone-climate interactions in the future. Future studies are needed to better understand how and to what extent these factors can influence the ozone-climate interactions. Additionally, we shall acknowledge several limitations in our study. Methodologically, reliance on model simulations

introduces inherent uncertainties. For example, changes in experimental conditions may affect the robustness of our results. A more complete solution to these limitations may require us to conduct longer historical simulation experiments in the future to

525 reduce experimental uncertainties. However, this study contributes to a better understanding of effects of ozone-climate interactions on the long-term temperature trend in the Arctic stratosphere, offering valuable insights for the development of climate models. Improved models could make a better predictions of stratospheric temperature changes, informing strategies for ozone protection and climate change mitigation.

Acknowledgments

530 This work is supported by the National Natural Science Foundation of China (U2442211, 42075062, 42130601). We also thank the scientific team at National Center for Atmospheric Research (NCAR) for providing the CESM-1 model. Finally, we thank the computing support provided by Supercomputing Center of Lanzhou University.

Author contributions

JZ provided ideas and formulation or evolution of overarching research goals and aims, SZ conducted experiments, produced
535 figures, and organized and wrote the paper. JZ, XX, CZ and ZW contributed to the revisions made to the paper. CZ also helped to design the experiments.

Competing interests

The contact author has declared that neither they nor their co-authors have any competing interests.

Date Availability Statement

540 The European Centre for Medium-Range Weather Forecasts (ECMWF) version 5 reanalysis dataset (ERA5) are openly available at https://cds.climate.copernicus.eu/cdsapp#!/dataset/reanalysis-era5-pressure-levels?tab=overview. The MERRA2 data are obtained from https://disc.gsfc.nasa.gov/datasets/M2I3NPASM_5.12.4/summary?keywords=%22MERRA-2%22. The CESM model is available at https://www2.cesm.ucar.edu/models/current. The data generated in this work can be obtained by contacting Siyi Zhao (120220900830@lzu.edu.cn).

References

545
Abalos, M., Randel, W. J., Kinnison, D. E., and Serrano, E.: Quantifying tracer transport in the tropical lower stratosphere using WACCM, Atmos. Chem. Phys., 13, 10591–10607, https://doi.org/10.5194/acp-13-10591-2013, 2013.

Albers, J. R. and Nathan, T. R.: Ozone Loss and Recovery and the Preconditioning of Upward-Propagating Planetary Wave Activity, J. Atmos. Sci., 70, 3977–3994, https://doi.org/10.1175/JAS-D-12-0259.1, 2013.

550   Andrews, D. G., Holton, J. R., and Leovy, C. B.: Middle atmosphere dynamics, Academic Press, Orlando, 489 pp., 1987.

Bohlinger, P., Sinnhuber, B.-M., Ruhnke, R., and Kirner, O.: Radiative and dynamical contributions to past and future Arctic stratospheric temperature trends, Atmos. Chem. Phys., 14, 1679–1688, https://doi.org/10.5194/acp-14-1679-2014, 2014.

Brasseur, G. and Solomon, S.: Aeronomy of the middle atmosphere: chemistry and physics of the stratosphere and mesosphere, 3rd rev. and enlarged ed., Springer, Dordrecht ; [Great Britain], 644 pp., 2005.

555   Calvo, N., Polvani, L. M., and Solomon, S.: On the surface impact of Arctic stratospheric ozone extremes, Environ. Res. Lett., 10, 094003, https://doi.org/10.1088/1748-9326/10/9/094003, 2015.

Chen, P. and Robinson, W. A.: Propagation of Planetary Waves between the Troposphere and Stratosphere, J. Atmos. Sci., 49, 2533–2545, https://doi.org/10.1175/1520-0469(1992)049<2533:POPWBT>2.0.CO;2, 1992.

Chiodo, G. and Polvani, L. M.: Reduction of Climate Sensitivity to Solar Forcing due to Stratospheric Ozone Feedback, Journal

560   of Climate, 29, 4651–4663, https://doi.org/10.1175/JCLI-D-15-0721.1, 2016.

Chiodo, G., Friedel, M., Seeber, S., Domeisen, D., Stenke, A., Sukhodolov, T., and Zilker, F.: The influence of future changes in springtime Arctic ozone on stratospheric and surface climate, Atmos. Chem. Phys., 23, 10451–10472, https://doi.org/10.5194/acp-23-10451-2023, 2023.

Chiodo, G., Liu, J., Revell, L., Sukhodolov, T., and Zhang, J.: Editorial: The Evolution of the Stratospheric Ozone, Frontiers

565   in Earth Science, 9, https://doi.org/10.3389/feart.2021.773826, 2021.

Chipperfield, M. P., Bekki, S., Dhomse, S., Harris, N. R. P., Hassler, B., Hossaini, R., Steinbrecht, W., Thiéblemont, R., and Weber, M.: Detecting recovery of the stratospheric ozone layer, Nature, 549, 211–218, https://doi.org/10.1038/nature23681, 2017.

Cohen, J., Screen, J. A., Furtado, J. C., Barlow, M., Whittleston, D., Coumou, D., Francis, J., Dethloff, K., Entekhabi, D.,

570   Overland, J., and Jones, J.: Recent Arctic amplification and extreme mid-latitude weather, Nature Geosci, 7, 627–637, https://doi.org/10.1038/ngeo2234, 2014.

Coy, L., Nash, E. R., and Newman, P. A.: Meteorology of the polar vortex: Spring 1997, Geophys. Res. Lett., 24, 2693–2696, https://doi.org/10.1029/97GL52832, 1997.

de F. Forster, P. M. and Shine, K. P.: Radiative forcing and temperature trends from stratospheric ozone changes, J. Geophys.

575   Res.-Atmos, 102, 10841–10855, https://doi.org/10.1029/96JD03510, 1997.

Dietmüller, S., Ponater, M., and Sausen, R.: Interactive ozone induces a negative feedback in CO_2 -driven climate change simulations, J. Geophys. Res.-Atmos., 119, 1796–1805, https://doi.org/10.1002/2013JD020575, 2014.

Eric Klobas, J., Wilmouth, D. M., Weisenstein, D. K., Anderson, J. G., and Salawitch, R. J.: Ozone depletion following future volcanic eruptions, Geophys. Res. Lett., 44, 7490–7499, https://doi.org/10.1002/2017GL073972, 2017.

580   Farman, J. C., Gardiner, B. G., and Shanklin, J. D.: Large losses of total ozone in Antarctica reveal seasonal ClOJNOx interaction, 1985.

Feng, W., Chipperfield, M. P., Roscoe, H. K., Remedios, J. J., Waterfall, A. M., Stiller, G. P., Glatthor, N., Höpfner, M., and Wang, D.-Y.: Three-Dimensional Model Study of the Antarctic Ozone Hole in 2002 and Comparison with 2000, J. Atmos. Sci., 62, 822–837, https://doi.org/10.1175/JAS-3335.1, 2005a.

585 Feng, W., Chipperfield, M. P., Davies, S., Sen, B., Toon, G., Blavier, J. F., Webster, C. R., Volk, C. M., Ulanovsky, A., Ravegnani, F., von der Gathen, P., Jost, H., Richard, E. C., and Claude, H.: Three-dimensional model study of the Arctic ozone loss in 2002/2003 and comparison with 1999/2000 and 2003/2004, Atmos. Chem. Phys., 5, 139–152, https://doi.org/10.5194/acp-5-139-2005, 2005b.

Friedel, M., Chiodo, G., Stenke, A., Domeisen, D. I. V., and Peter, T.: Effects of Arctic ozone on the stratospheric spring onset
590 and its surface impact, Atmos. Chem. Phys., 22, 13997–14017, https://doi.org/10.5194/acp-22-13997-2022, 2022a.

Friedel, M., Chiodo, G., Stenke, A., Domeisen, D. I. V., Fueglistaler, S., Anet, J. G., and Peter, T.: Springtime arctic ozone depletion forces northern hemisphere climate anomalies, Nat. Geosci., 15, 541–547, https://doi.org/10.1038/s41561-022-00974-7, 2022b.

Friedel, M., Chiodo, G., Sukhodolov, T., Keeble, J., Peter, T., Seeber, S., Stenke, A., Akiyoshi, H., Rozanov, E., Plummer, D.,
595 Jöckel, P., Zeng, G., Morgenstern, O., and Josse, B.: Weakening of springtime Arctic ozone depletion with climate change, Atmos. Chem. Phys., 23, 10235–10254, https://doi.org/10.5194/acp-23-10235-2023, 2023.

Fu, Q., Solomon, S., Pahlavan, H. A., and Lin, P.: Observed changes in Brewer–Dobson circulation for 1980–2018, Environ. Res. Lett., 14, 114026, https://doi.org/10.1088/1748-9326/ab4de7, 2019.

Gelaro, R., McCarty, W., Suárez, M. J., Todling, R., Molod, A., Takacs, L., Randles, C. A., Darmenov, A., Bosilovich, M. G.,
600 Reichle, R., Wargan, K., Coy, L., Cullather, R., Draper, C., Akella, S., Buchard, V., Conaty, A., Da Silva, A. M., Gu, W., Kim, G.-K., Koster, R., Lucchesi, R., Merkova, D., Nielsen, J. E., Partyka, G., Pawson, S., Putman, W., Rienecker, M., Schubert, S. D., Sienkiewicz, M., and Zhao, B.: The Modern-Era Retrospective Analysis for Research and Applications, Version 2 (MERRA-2), J. Climate, 30, 5419–5454, https://doi.org/10.1175/JCLI-D-16-0758.1, 2017.

Haase, S. and Matthes, K.: The importance of interactive chemistry for stratosphere–troposphere coupling, Atmos. Chem.
605 Phys., 19, 3417–3432, https://doi.org/10.5194/acp-19-3417-2019, 2019.

Haynes, P. H., McIntyre, M. E., Shepherd, T. G., Marks, C. J., and Shine, K. P.: On the "Downward Control" of Extratropical Diabatic Circulations by Eddy-Induced Mean Zonal Forces, J. Atmos. Sci., 48, 651–678, https://doi.org/10.1175/1520-0469(1991)048<0651:OTCOED>2.0.CO;2, 1991.

Hersbach, H., Bell, B., Berrisford, P., Hirahara, S., Horányi, A., Muñoz‐Sabater, J., Nicolas, J., Peubey, C., Radu, R.,
610 Schepers, D., Simmons, A., Soci, C., Abdalla, S., Abellan, X., Balsamo, G., Bechtold, P., Biavati, G., Bidlot, J., Bonavita, M., De Chiara, G., Dahlgren, P., Dee, D., Diamantakis, M., Dragani, R., Flemming, J., Forbes, R., Fuentes, M., Geer, A., Haimberger, L., Healy, S., Hogan, R. J., Hólm, E., Janisková, M., Keeley, S., Laloyaux, P., Lopez, P., Lupu, C., Radnoti, G., De Rosnay, P., Rozum, I., Vamborg, F., Villaume, S., and Thépaut, J.: The ERA5 global reanalysis, Q. J. Roy. Meteor. Soc., 146, 1999–2049, https://doi.org/10.1002/qj.3803, 2020.

Hu, D. and Guan, Z.: Relative Effects of the Greenhouse Gases and Stratospheric Ozone Increases on Temperature and Circulation in the Stratosphere over the Arctic, Remote Sensing, 14, 3447, https://doi.org/10.3390/rs14143447, 2022.

Hu, D., Guan, Z., and Tian, W.: Signatures of the Arctic Stratospheric Ozone in Northern Hadley Circulation Extent and Subtropical Precipitation, Geophys. Res. Lett., 46, 12340–12349, https://doi.org/10.1029/2019GL085292, 2019a.

Hu, D., Guo, Y., and Guan, Z.: Recent Weakening in the Stratospheric Planetary Wave Intensity in Early Winter, Geophys. Res. Lett., 46, 3953–3962, https://doi.org/10.1029/2019GL082113, 2019b.

Hu, D., Tian, W., Xie, F., Wang, C., and Zhang, J.: Impacts of stratospheric ozone depletion and recovery on wave propagation in the boreal winter stratosphere, J. Geophys. Res.-Atmos., 120, 8299–8317, https://doi.org/10.1002/2014JD022855, 2015.

Hu, Y. and Fu, Q.: Stratospheric warming in Southern Hemisphere high latitudes since 1979, Atmos. Chem. Phys., 9, 4329–4340, https://doi.org/10.5194/acp-9-4329-2009, 2009.

Hu, Y., Tian, W., Zhang, J., Wang, T., and Xu, M.: Weakening of Antarctic stratospheric planetary wave activities in early austral spring since the early 2000s: a response to sea surface temperature trends, Atmos. Chem. Phys., 22, 1575–1600, https://doi.org/10.5194/acp-22-1575-2022, 2022.

Hu, Y. and Tung, K. K.: Possible Ozone-Induced Long-Term Changes in Planetary Wave Activity in Late Winter, J. Climate, 16, 3207–3038, https://doi.org/10.1175/1520-0442(2003)016<3027:POLCIP>2.0.CO;2, 2003.

Huang, J., Tian, W., Gray, L. J., Zhang, J., Li, Y., Luo, J., and Tian, H.: Preconditioning of Arctic Stratospheric Polar Vortex Shift Events, Journal of Climate, 31, 5417–5436, https://doi.org/10.1175/JCLI-D-17-0695.1, 2018.

IPCC 2014: Intergovernmental Panel on Climate Change: Climate change 2014: mitigation of climate change: Working Group III contribution to the Fifth Assessment Report of the Intergovernmental Panel on Climate Change, Cambridge University Press, New York, NY, 2014.

IPCC 2021: Intergovernmental Panel on Climate Change: Climate Change 2021: The Physical Science Basis. Contribution of Working Group I to the Sixth Assessment Report of the Intergovernmental Panel on Climate Change. Cambridge University Press, Cambridge, United Kingdom and New York, NY, USA, 2021.

Ivanciu, I., Matthes, K., Biastoch, A., Wahl, S., and Harlaß, J.: Twenty-first-century Southern Hemisphere impacts of ozone recovery and climate change from the stratosphere to the ocean, Weather Clim. Dynam., 3, 139–171, https://doi.org/10.5194/wcd-3-139-2022, 2022.

Lin, P. and Ming, Y.: Enhanced Climate Response to Ozone Depletion From Ozone‐Circulation Coupling, J. Geophys. Res.-Atmos., 126, e2020JD034286, https://doi.org/10.1029/2020JD034286, 2021.

Marsh, D. R., Lamarque, J., Conley, A. J., and Polvani, L. M.: Stratospheric ozone chemistry feedbacks are not critical for the determination of climate sensitivity in CESM1(WACCM), Geophys. Res. Lett., 43, 3928–3934, https://doi.org/10.1002/2016GL068344, 2016.

Matsuno, T.: Vertical Propagation of Stationary Planetary Waves in the Winter Northern Hemisphere, J. Atmos. Sci., 27, 871–883, https://doi.org/10.1175/1520-0469(1970)027<0871:VPOSPW>2.0.CO;2, 1970.

Meul, S., Dameris, M., Langematz, U., Abalichin, J., Kerschbaumer, A., Kubin, A., and Oberländer‑Hayn, S.: Impact of rising greenhouse gas concentrations on future tropical ozone and UV exposure, Geophys. Res. Lett., 43, 2919–2927, https://doi.org/10.1002/2016GL067997, 2016.

Mitchell, D. M., Charlton-Perez, A. J., and Gray, L. J.: Characterizing the Variability and Extremes of the Stratospheric Polar Vortices Using 2D Moment Analysis, J. Atmos. Sci., 68, 1194–1213, https://doi.org/10.1175/2010JAS3555.1, 2011.

Monier, E. and Weare, B. C.: Climatology and trends in the forcing of the stratospheric ozone transport, Atmos. Chem. Phys., 11, 6311–6323, https://doi.org/10.5194/acp-11-6311-2011, 2011.

Nakamura, M., Kadota, M., and Yamane, S.: Quasigeostrophic Transient Wave Activity Flux: Updated Climatology and Its Role in Polar Vortex Anomalies, J. Atmos. Sci., 67, 3164–3189, https://doi.org/10.1175/2010JAS3451.1, 2010.

Nathan, T. R. and Cordero, E. C.: An ozone‑modified refractive index for vertically propagating planetary waves, J. Geophys. Res.-Atmos., 112, 2006JD007357, https://doi.org/10.1029/2006JD007357, 2007.

Neale, R. B., Richter, J., Park, S., Lauritzen, P. H., Vavrus, S. J., Rasch, P. J., and Zhang, M.: The Mean Climate of the Community Atmosphere Model (CAM4) in Forced SST and Fully Coupled Experiments, J. Climate, 26, 5150–5168, https://doi.org/10.1175/JCLI-D-12-00236.1, 2013.

Newman, P. A., Daniel, J. S., Waugh, D. W., and Nash, E. R.: A new formulation of equivalent effective stratospheric chlorine (EESC), Atmos. Chem. Phys., 7, 4537–4552, https://doi.org/10.5194/acp-7-4537-2007, 2007.

Newman, P. A., Nash, E. R., and Rosenfield, J. E.: What controls the temperature of the Arctic stratosphere during the spring?, J. Geophys. Res.-Atmos., 106, 19999–20010, https://doi.org/10.1029/2000JD000061, 2001.

Nowack, P. J., Luke Abraham, N., Maycock, A. C., Braesicke, P., Gregory, J. M., Joshi, M. M., Osprey, A., and Pyle, J. A.: A large ozone-circulation feedback and its implications for global warming assessments, Nat. Clim. Change, 5, 41–45, https://doi.org/10.1038/nclimate2451, 2015.

Ossó, A., Sola, Y., Rosenlof, K., Hassler, B., Bech, J., and Lorente, J.: How Robust Are Trends in the Brewer–Dobson Circulation Derived from Observed Stratospheric Temperatures?, J. Climate, 28, 3204–3040, https://doi.org/10.1175/JCLI-D-14-00295.1, 2015.

Overland, J. E., Dethloff, K., Francis, J. A., Hall, R. J., Hanna, E., Kim, S.-J., Screen, J. A., Shepherd, T. G., and Vihma, T.: Nonlinear response of mid-latitude weather to the changing Arctic, Nature Clim Change, 6, 992–999, https://doi.org/10.1038/nclimate3121, 2016.

Randel, W. J. and Wu, F.: Changes in Column Ozone Correlated with the Stratospheric EP Flux, J. Meteorol Soc. JPN., 80, 849–862, https://doi.org/10.2151/jmsj.80.849, 2002.

Ravishankara, A. R., Daniel, J. S., and Portmann, R. W.: Nitrous Oxide (N_2O): The Dominant Ozone-Depleting Substance Emitted in the 21st Century, Science, 326, 123–125, https://doi.org/10.1126/science.1176985, 2009.

Revell, L. E., Tummon, F., Salawitch, R. J., Stenke, A., and Peter, T.: The changing ozone depletion potential of N_2O in a future climate, Geophys. Res. Lett., 42, https://doi.org/10.1002/2015GL065702, 2015.

Rieder, H. E., Chiodo, G., Fritzer, J., Wienerroither, C., and Polvani, L. M.: Is interactive ozone chemistry important to represent polar cap stratospheric temperature variability in Earth-System Models?, Environ. Res. Lett., 14, 044026, https://doi.org/10.1088/1748-9326/ab07ff, 2019.

685   Screen, J. A. and Simmonds, I.: The central role of diminishing sea ice in recent Arctic temperature amplification, Nature, 464, 1334–1337, https://doi.org/10.1038/nature09051, 2010.

Seppälä, A., Kalakoski, N., Verronen, P. T., Marsh, D. R., Karpechko, A. Yu., and Szelag, M. E.: Polar mesospheric ozone loss initiates downward coupling of solar signal in the Northern Hemisphere, Nat Commun, 16, 748, https://doi.org/10.1038/s41467-025-55966-z, 2025.

690   Serreze, M. C. and Barry, R. G.: Processes and impacts of Arctic amplification: A research synthesis, Global and Planetary Change, 77, 85–96, https://doi.org/10.1016/j.gloplacha.2011.03.004, 2011.

Shindell, D. and Faluvegi, G.: Climate response to regional radiative forcing during the twentieth century, Nature Geosci, 2, 294–300, https://doi.org/10.1038/ngeo473, 2009.

Sigmond, M. and Fyfe, J. C.: The Antarctic Sea Ice Response to the Ozone Hole in Climate Models, J. Climate, 27, 1336–
695   1342, https://doi.org/10.1175/JCLI-D-13-00590.1, 2014.

Simpson, I. R., Blackburn, M., and Haigh, J. D.: The Role of Eddies in Driving the Tropospheric Response to Stratospheric Heating Perturbations, J. Atmos. Sci., 66, 1347–1365, https://doi.org/10.1175/2008JAS2758.1, 2009.

Smith, K. L. and Polvani, L. M.: The surface impacts of Arctic stratospheric ozone anomalies, Environ. Res. Lett., 9, 074015, https://doi.org/10.1088/1748-9326/9/7/074015, 2014.

700   Solomon, S., Garciat, R. R., Rowland, F. S., and Wuebbles, D. J.: On the depletion of Antarctic ozone, Nature, 321,755–758, https://doi.org/10.1038/321755a0, 1986.

Solomon, S., Plattner, G.-K., Knutti, R., and Friedlingstein, P.: Irreversible climate change due to carbon dioxide emissions, Proc. Natl. Acad. Sci. U.S.A., 106, 1704–1709, https://doi.org/10.1073/pnas.0812721106, 2009.

Son, S.-W., Polvani, L. M., Waugh, D. W., Akiyoshi, H., Garcia, R., Kinnison, D., Pawson, S., Rozanov, E., Shepherd, T. G.,
705   and Shibata, K.: The Impact of Stratospheric Ozone Recovery on the Southern Hemisphere Westerly Jet, Science, 320, 1486–1489, https://doi.org/10.1126/science.1155939, 2008.

Song, B.-G. and Chun, H.-Y.: Residual Mean Circulation and Temperature Changes during the Evolution of Stratospheric Sudden Warming Revealed in MERRA, acp.copernicus.org [preprints], https://doi.org/10.5194/acp-2016-729, 15 November 2016.

710   SPARC LOTUS Activity: SPARC/IO3C/GAW Report on Long-term Ozone Trends and Uncertainties in the Stratosphere. World Climate Research Programme, 2019. 102 p. (SPARC Reports). https://doi.org/10.17874/f899e57a20b, 2019.

Takaya, K. and Nakamura, H.: A formulation of a wave‑activity flux for stationary Rossby waves on a zonally varying basic flow, Geophys. Res. Lett., 24, 2985–2988, https://doi.org/10.1029/97GL03094, 1997.

Takaya, K. and Nakamura, H.: A Formulation of a Phase-Independent Wave-Activity Flux for Stationary and Migratory Quasigeostrophic Eddies on a Zonally Varying Basic Flow, J. Atmos. Sci., 58, 608–627, https://doi.org/10.1175/1520-0469(2001)058<0608:AFOAPI>2.0.CO;2, 2001.

Tett, S. F. B., Mitchell, J. F. B., Parker, D. E., and Allen, M. R.: Human Influence on the Atmospheric Vertical Temperature Structure: Detection and Observations, Science, 274, 1170–1173, https://doi.org/10.1126/science.274.5290.1170, 1996.

Tian, W., Huang, J., Zhang, J., Xie, F., Wang, W., and Peng, Y.: Role of Stratospheric Processes in Climate Change: Advances and Challenges, Adv. Atmos. Sci., 40, 1379–1400, https://doi.org/10.1007/s00376-023-2341-1, 2023.

WMO: Scientific Assessment of Ozone Depletion: 2022: https://library.wmo.int/records/item/58360-scientific-assessment-of-ozone-depletion-2022?language_id=13&back=&offset=2, last access: 5 July 2024.

Xia, Y., Hu, Y., and Huang, Y.: Strong modification of stratospheric ozone forcing by cloud and sea-ice adjustments, Atmos. Chem. Phys., 16, 7559–7567, https://doi.org/10.5194/acp-16-7559-2016, 2016.

Xie, F., Ma, X., Li, J., Huang, J., Tian, W., Zhang, J., Hu, Y., Sun, C., Zhou, X., Feng, J., and Yang, Y.: An advanced impact of Arctic stratospheric ozone changes on spring precipitation in China, Clim. Dyn., 51, 4029–4041, https://doi.org/10.1007/s00382-018-4402-1, 2018.

Young, P. J., Rosenlof, K. H., Solomon, S., Sherwood, S. C., Fu, Q., and Lamarque, J.-F.: Changes in Stratospheric Temperatures and Their Implications for Changes in the Brewer–Dobson Circulation, 1979–2005, J. Climate, 25, 1759–1772, https://doi.org/10.1175/2011JCLI4048.1, 2012.

Zhang, J., Tian, W., Chipperfield, M. P., Xie, F., and Huang, J.: Persistent shift of the Arctic polar vortex towards the Eurasian continent in recent decades, Nat. Clim. Change, 6, 1094–1099, https://doi.org/10.1038/nclimate3136, 2016.

Zhang, J., Tian, W., Xie, F., Pyle, J. A., Keeble, J., and Wang, T.: The Influence of Zonally Asymmetric Stratospheric Ozone Changes on the Arctic Polar Vortex Shift, J. Climate, 33, 4641–4658, https://doi.org/10.1175/JCLI-D-19-0647.1, 2020.

Zhang, J., Xie, F., Ma, Z., Zhang, C., Xu, M., Wang, T., and Zhang, R.: Seasonal Evolution of the Quasi‑biennial Oscillation Impact on the Northern Hemisphere Polar Vortex in Winter, J. Geophys. Res.-Atmos., 124, 12568–12586, https://doi.org/10.1029/2019JD030966, 2019.

Zhang, J., Xie, F., Tian, W., Han, Y., Zhang, K., Qi, Y., Chipperfield, M., Feng, W., Huang, J., and Shu, J.: Influence of the Arctic Oscillation on the Vertical Distribution of Wintertime Ozone in the Stratosphere and Upper Troposphere over the Northern Hemisphere, J. Climate, 30, 2905–2919, https://doi.org/10.1175/JCLI-D-16-0651.1, 2017.

Zhao, S., Zhang, J., Zhang, C., Xu, M., Keeble, J., Wang, Z., and Xia, X.: Evaluating Long-Term Variability of the Arctic Stratospheric Polar Vortex Simulated by CMIP6 Models, Remote Sens., 14, 4701, https://doi.org/10.3390/rs14194701, 2022.

Zhou, S., Miller, A. J., Wang, J., and Angell, J. K.: Trends of NAO and AO and their associations with stratospheric processes, Geophys. Res. Lett., 28, 4107–4110, https://doi.org/10.1029/2001GL013660, 2001.